Hemizygous Mutation of the Peripheral Myelin Protein 22 Gene Associated with Charcot-Marie-Tooth Disease Type 1

Chikahiko Numakura, MD,* Changqing Lin, MD,* Nobuyuki Oka, MD, PhD,† Ichiro Akiguchi, MD, PhD,† and Kiyoshi Hayasaka, MD, PhD*

We studied a female patient who presented with autosomal recessive or sporadic Charcot-Marie-Tooth disease type 1 (CMT1). We found that she had a 1.5-megabase deletion in chromosome 17p11.2–p12 containing the peripheral myelin protein 22 gene (*PMP22*) and an Arg157Gly mutation of *PMP22*. Hemizygous mutation of *PMP22* should be considered in patients with autosomal recessive CMT1 or with severe hereditary neuropathy with liability to pressure palsy.

Numakura C, Lin C, Oka N, Akiguchi I, Hayasaka K. Hemizygous mutation of the peripheral myelin protein 22 gene associated with Charcot-Marie-Tooth disease type 1. Ann Neurol 2000;47:101–103

Charcot-Marie-Tooth neuropathy type 1A (CMT1A) is a genetically heterogenous peripheral neuropathy and is characterized clinically by distal muscle weakness and atrophy, absence of deep tendon reflexes, and pes cavus deformity of the feet.[1] Most CMT1A patients have a 1.5-megabase (Mb) duplication in chromosome 17p11.2–p12, including the peripheral myelin protein 22 gene (*PMP22*),[2,3] and some of them have point mutations of *PMP22*.[4] CMT1A is an autosomal dominant neuropathy; however, a patient who was compound heterozygous for a recessive Thr118Met mutation of *PMP22* and a 1.5-Mb deletion in chromosome 17p11.2–p12 was reported as having autosomal recessive CMT1A.[5] Recently, Parman and co-workers[6] reported that 3 siblings with Dejerine-Sottas disease, a severe form of CMT1, showed a recessive pattern of inheritance of an Arg157Trp mutation of *PMP22*. In this study, we report a patient with CMT1 who was compound heterozygous for an Arg157Gly mutation of *PMP22* and a 1.5-Mb deletion in chromosome 17p11.2–p12.

From the *Department of Pediatrics, Yamagata University School of Medicine, Yamagata, and †Department of Neurology, Kyoto University Hospital, Kyoto, Japan.

Received Jun 23, 1999, and in revised form Aug 5. Accepted for publication Aug 5, 1999.

Address correspondence to Dr Hayasaka, Department of Pediatrics, Yamagata University School of Medicine, Yamagata 990-9585, Japan.

Subject and Methods

Subject

A 57-year-old woman had shown slowly progressive muscular weakness and atrophy of the distal extremities since the age of 20 years. On examination, she showed severe claw hands and pes cavus. All modalities of sensation were impaired in the distal extremities. Motor nerve conduction velocities were decreased and showed no asymmetry (median: R = 22 m/sec, L = 18 m/sec; tibial: R = 22 m/sec, L = 24 m/sec). No conduction blocks were found. Her parents, son, and 6 siblings did not show any signs of peripheral neuropathy.

Analysis of a 1.5-Mb Duplication or Deletion in Chromosome 17p11.2–p12

Genomic DNA was extracted from peripheral blood leukocytes of the patient and healthy controls. To test for a 1.5-Mb duplication or deletion in chromosome 17p11.2–p12, we performed Southern blot analysis using a pHK1.0P probe, which detects 2.3- and 3.2-kilobase (kb) EcoRI DNA fragments. The radioactivity of those fragments was measured with a photostimulated luminescence imaging plate, and the radioactivity ratio of 2.3:3.2 kb was calculated as described.[7] The ratios for controls, patients with a duplication, and patients with a deletion were 1.0 ± 0.0 (mean ± SD; n = 10), 1.6 ± 0.1 (mean ± SD; n = 6), and 0.5 ± 0.1 (mean ± SD; n = 8), respectively.

Single-Strand Conformation Polymorphism Analysis of the PMP22 *Gene, the Myelin Protein Zero Gene, and the Connexin 32 Gene*

All coding regions of *PMP22*, the myelin protein zero gene (*Po*), and the connexin 32 gene (*Cx32*) were amplified by polymerase chain reaction and used for single-strand conformation polymorphism (SSCP) analysis. SSCP analyses for *PMP22* and *Cx32* were done as described.[4,8,9] For *Po* analysis, six primer sets were designed by means of genomic information[10]:

Exon 1: SS1F = 5′-CCCGTTCAGTTCCTGGT-3′ and SS1R = 5′-AGACACCTGAGTCCCAAGAC-3′
Exon 2: SS2F = 5′-CCATAGGTGCATCTGATTCC-3′ and SS2R = 5′-TCTGTTATCCAACCCCAGGA-3′
Exon 3: SS3F = 5′-TCATTAGGGTCCTCTCACATGC-3′ and SS3R 5′-AACTGCTTCCCATACCCTTG-3′
Exon 4: SS4F = 5′-CTGCTCATTCTCCCACTTCT-3′ and SS4R = 5′-ACCCACTGGAGTAGTCT-3′
Exon 5: SS5F = 5′-CGCGGTGCAAGGGGTTCC-3′ and SS5R = 5′-GGGTTCTCCTTCCCATC-3′
Exon 6: SS6F = 5′-TCGCTCGGTGACTGATGTG-3′ and SS6R = 5′-AGGCCCATCATGTTCTTGAG-3′

Sequence Analysis

The sequence determination of exon 5 of *PMP22* was performed on an ABI PRISM 310 Genetic Analyzer (Applied

Biosystems, Foster City, CA) using polymerase chain reaction products amplified with primers as previously described.[8] Nucleotide numbering of coding regions was according to the method of Hayasaka and colleagues[11]

Morphological Study

Pathological examination of a sural nerve biopsy was performed as described previously.[12]

Results

Light microscopy showed a markedly decreased number of large myelinated fibers (myelinated fiber density = 2,756/mm^2, control = 6,720–8,560/mm^2; n = 6). Hypermyelinated fibers were prominent, and electron microscopy showed excessive outfolding and infolding (Fig 1). Regenerating clusters were frequent (53/mm^2), but onion bulb formations were rare. A teased nerve fiber study showed tomaculae with variable myelin thickness in 18% of the fibers. Decreased myelinated fiber density and increased regenerating clusters were different from those typically observed in patients with hereditary neuropathy with liability to pressure palsy (HNPP).[13]

Southern blot analysis was performed to detect a 1.5-Mb duplication in chromosome 17p11.2–p12. The radioactivity ratio (2.3:3.2 kb) was 0.4 instead of 1.5, which meant a 1.5-Mb deletion in chromosome 17p11.2–p12.

In addition, SSCP analysis of *PMP22*, *Po*, and *Cx32* only showed an abnormal pattern in the fragment that included exon 5 of *PMP22*. Sequence analysis revealed a C-to-G mutation at nucleotide position 657, leading to an Arg157Gly substitution in the intracellular domain of *PMP22* (Fig 2). The patient was compound heterozygous for a 1.5-Mb deletion in chromosome 17p11.2–p12 and an Arg157Gly mutation of *PMP22*.

Fig 1. Electron micrograph of the sural nerve from the patient shows excessive outfolding and infolding of myelinated fibers.

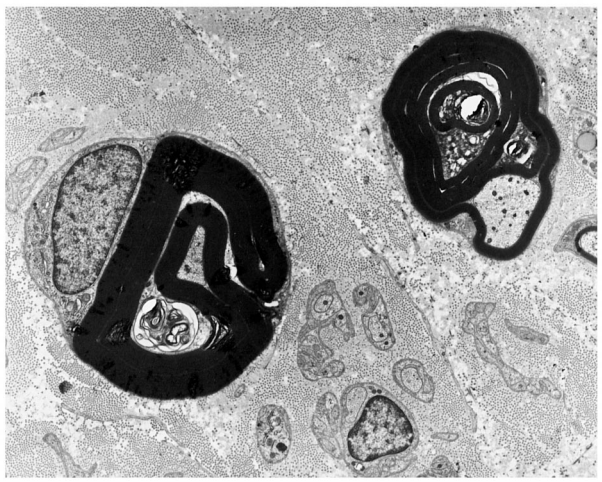

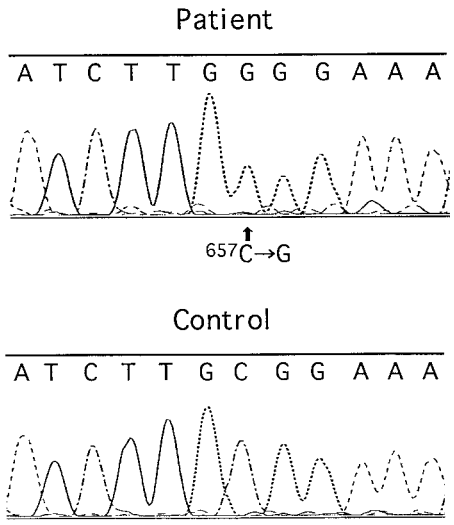

Fig 2. Sequence chromatogram of the patient shows a C-to-G mutation at nucleotide 657 (arrow) *of the PMP22 gene, which results in an Arg157Gly substitution. Only the mutant G-allele is present, and no heterozygous band is observed for the wild-type allele because of the hemizygous state as a result of the hereditary neuropathy with liability to pressure palsy–related deletion on the other chromosome.*

Discussion

Most patients with CMT1A have a 1.5-Mb duplication in chromosome 17p11.2–p12 containing *PMP22*.[2,3] A reciprocal 1.5-Mb deletion in chromosome 17p11.2–p12 is associated with HNPP, which is an autosomal dominant inherited disorder with episodic, recurrent, and pressure-induced peripheral neuropathy.[14] Several point mutations of *PMP22* have been identified in nonduplicated CMT1A patients[4] or nondeleted HNPP patients.[15] It is currently postulated that overexpression of PMP22 as the result of a duplication in chromosome 17p11.2–p12 or mutated PMP22, which may act in a dominant-negative manner or be toxic to Schwann cells (gain of function), is associated with CMT1A. Conversely, decreased expression of PMP22 as the result of a deletion in chromosome 17p11.2–p12 or mutated PMP22, which may lead to a loss of function, causes HNPP. The clinical heterogeneity of CMT1 is well known; however, symptoms would essentially be determined by the manner of impairment of the candidate genes.

Parman and co-workers[6] recently reported that a recessive Arg157Trp mutation of *PMP22* was associated with Dejerine-Sottas disease. Heterozygotes of this mutation were asymptomatic with normal nerve conduction velocities. Our mutation was also located at Arg157 and was not detected in 100 healthy controls. No other family members had any problems in their daily life. Although we cannot deny the possibility of de novo mutation or misunderstanding of paternity,

the Arg157Gly mutation seems to be harmless in a heterozygous state. Unfortunately, genetic information on the family members of our patient was not available.

Roa and associates[5] described a patient who was compound heterozygous for a Thr118Met mutation of *PMP22* and a 1.5-Mb deletion in chromosome 17p11.2–p12 as having autosomal recessive CMT1. Nelis and co-workers[16] detected the Thr118Met mutation in a heterozygous state in 10 control individuals and suspected the Thr118Met mutation to be a harmless polymorphism. They did not detect the mutation in a homozygous or hemizygous state, however. Considering the patients with a hemizygous Arg157Gly mutation, it is likely that hemizygous Thr118Met mutation is not a harmless polymorphism but a recessive mutation. The detection of more patients carrying the same mutation or the development of a mouse model would help us to understand the implications of the mutation and its pathogenesis.

There have been reports of severe cases of HNPP.[17] We usually consider the goal of molecular diagnosis in HNPP patients to be the detection of a heterozygous 1.5-Mb deletion in chromosome 17p11.2–p12. We should also check *PMP22* of the other allele in severe cases. We should also evaluate *PMP22* in cases of autosomal recessive CMT1.

This work was supported in part by grants from the Ministry of Education, Science and Culture and by grants for Pediatric Research and Hereditary Neuropathies from the Ministry of Health and Welfare, Japan.

References

1. Dyck PJ, Chance P, Lebo R, Carney JA. Hereditary motor and sensory neuropathies. In: Dyck PJ, Thomas PK, Griffin JW, et al, eds. Peripheral neuropathy. Philadelphia: WB Saunders, 1993:1096–1113
2. Lupski JR, de Oca-Luna RM, Slaugenhaupt S, et al. DNA duplication associated with Charcot-Marie-Tooth disease type 1A. Cell 1991;66:219–232
3. Raeymaekers P, Timmerman V, Nelis E, et al. Duplication in chromosome 17p11.2 in Charcot-Marie-Tooth neuropathy type 1a (CMT 1a). The HMSN Collaborative Research Group. Neuromuscul Disord 1991;1:93–97
4. Roa BB, Garcia CA, Suter U, et al. Charcot-Marie-Tooth disease type 1A. Association with a spontaneous point mutation in the PMP22 gene. N Engl J Med 1993;329:96–101
5. Roa BB, Garcia CA, Pentao L, et al. Evidence for a recessive PMP22 point mutation in Charcot-Marie-Tooth disease type 1A. Nat Genet 1993;5:189–194
6. Parman Y, Plante-Bordeneuve V, Guiochon-Mantel A, et al. Recessive inheritance of a new point mutation of the PMP22 gene in Dejerine-Sottas disease. Ann Neurol 1999;45:518–522
7. Ikegami T, Ikeda H, Chance PF, et al. Facilitated diagnosis of CMT1A duplication in chromosome 17p11.2–12: analysis with a CMT1A-REP repeat probe and photostimulated luminescence imaging. Hum Mutat 1997;9:563–566
8. Ikegami T, Ikeda H, Aoyama M, et al. Novel mutations of the peripheral myelin protein 22 gene in two pedigrees with Dejerine-Sottas disease. Hum Genet 1998;102:294–298
9. Yoshimura T, Ohnishi A, Yamamoto T, et al. Two novel mutations (C53S, S26L) in the connexin32 of Charcot-Marie-Tooth disease type X families. Hum Mutat 1996;8:270–272
10. Hayasaka K, Himoro M, Wang Y, et al. Structure and chromosomal localization of the gene encoding the human myelin protein zero (MPZ). Genomics 1993;17:755–758
11. Hayasaka K, Himoro M, Nanao K, et al. Isolation and sequence determination of cDNA encoding PMP-22 (PAS-II/SR13/Gas-3) of human peripheral myelin. Biochem Biophys Res Commun 1992;186:827–831
12. Kaji R, Oka N, Tsuji T, et al. Pathological findings at the site of conduction block in multifocal motor neuropathy. Ann Neurol 1993;33:152–158
13. Windebank AJ. Inherited recurrent focal neuropathies. In: Dyck PJ, Thomas PK, Griffin JW, et al, eds. Peripheral neuropathy. Philadelphia: WB Saunders, 1993:1137–1148
14. Chance PF, Alderson MK, Leppig KA, et al. DNA deletion associated with hereditary neuropathy with liability to pressure palsies. Cell 1993;72:143–151
15. Nicholson GA, Valentijn LJ, Cherryson AK, et al. A frame shift mutation in the PMP22 gene in hereditary neuropathy with liability to pressure palsies. Nat Genet 1994;6:263–266
16. Nelis E, Holmberg B, Adolfsson R, et al. PMP22 Thr(118)Met: recessive CMT1 mutation or polymorphism? Nat Genet 1997;15:13–14
17. Pareyson D, Scaioli V, Taroni F, et al. Phenotypic heterogeneity in hereditary neuropathy with liability to pressure palsies associated with chromosome 17p11.2–12 deletion. Neurology 1996;46:1133–1137

Clinical and Magnetic Resonance Imaging Findings in Chronic Sensory Ganglionopathies

Giuseppe Lauria, MD,* Davide Pareyson, MD,*
Marina Grisoli, MD,† and Angelo Sghirlanzoni, MD*

Twenty-two of 29 patients with chronic sensory ataxic neuropathy showed T2-weighted magnetic resonance imaging high signal intensity in the posterior columns of the cervical spine. T2 changes reflected the degeneration of central sensory projections and localized the disease process to T-shaped dorsal root ganglion neurons. No similar abnormalities were found in sensory and sensorimotor length-dependent axonal neuropathy patients. Spinal cord magnetic resonance imaging is a useful tool to support the clinical diagnosis of primary ganglionopathy.

Lauria G, Pareyson D, Grisoli M, Sghirlanzoni A.
Clinical and magnetic resonance imaging findings
in chronic sensory ganglionopathies.
Ann Neurol 2000;47:104–109

Axonal sensory neuropathies are often classified by the functional involvement of distinct fiber classes.[1] A further diagnostic approach is based on the determination of the major site of pathology and appears particularly useful in the differential diagnosis between sensory axonal and ganglionic neuropathies, in which routine clinical and electrophysiological evaluation alone often do not provide definite clues.[2]

Magnetic resonance imaging (MRI) high signal intensity in the posterior columns of the spinal cord, reflecting the degeneration of central sensory projections in primary dorsal root ganglia (DRG) impairment, was reported in a limited number of patients.[3–5] We correlated clinical and electrophysiological features with MRI findings in 29 patients with chronic ataxic neuropathy, aiming to support the diagnosis of sensory ganglionopathy.

Patients and Methods

Twenty-nine patients, referred to our Institute for predominantly sensory disturbances, were evaluated. Patients with demyelinating polyneuropathy or with residual sensory ataxia from Guillain-Barré syndrome were excluded. All patients underwent complete neurological evaluation, standard electrophysiological study, somatosensory evoked potential recording by stimulating tibial and median nerves, and cervical spine MRI on a 1.5-T unit (ACS II, Philips, Best, The Netherlands). Axial T2-weighted gradient echo images (repetition time [TR], 500 msec; echo time [TE], 9 msec; flip angle, 20°; slice thickness, 4 mm; field of view, 230 mm) were obtained in all patients. Two patients also underwent thoracic and lumbar MRI scanning. Three patients with severe diabetic and familial amyloid sensorimotor axonal neuropathy were submitted to cervical MRI scanning, as a control group. Radiological, hematological, biochemical, and serological screening was performed to disclose malignancies and thyroid, connective, infectious, metabolic, and vitamin disorders. Anti-nuclear, anti–smooth muscle, anti-mitochondrial, anti-dsDNA, anti–myelin-associated glycoprotein, and anti-Hu antibodies were assayed. Cerebrospinal fluid was analyzed in 19 patients. In selected cases, molecular genetic analyses for mitochondrial diseases, spinocerebellar and Friedreich ataxia, and nerve, muscle, and skin biopsy[6] were performed.

Results

Neurological Features

Disease onset was insidious in all patients except Patients 8 and 11, who experienced subacute limb hyperalgia and ataxia. Gait unsteadiness and proprioceptive sensory loss dominated the clinical picture (Table). The distribution of the most severe involvement varied from severe trunk and limb ataxia, which made Patient 10 unable to stand and walk, to pseudoathetosis and inability to localize in space only one arm (Patient 6). Nineteen patients complained of positive sensory symptoms (paresthesia, dysesthesia, hyperesthesia, allodynia, burning, or shooting pain) at the extremities, in most cases associated with light touch, pain, and temperature sensory loss. In 7 patients (Patients 4–10), cutaneous sensory dysfunctions were asymmetrically distributed, and in most of them also involved face or trunk either at the onset or in the course of the disease. Deep tendon reflexes were generally reduced or absent, except for Patient 22 who was hyperreflexic. Three patients (Patients 1, 2, and 5) showed nystagmus and depressed vestibular reflexes. Adie's pupils were observed in 2 patients (Patients 6 and 7) and were associated with sexual dysfunction in 1 case (Patient 8), whereas 2 patients (Patients 9 and 10) had intestinal pseudoobstruction probably related to myenteric plexus impairment. Strength examination was normal in all patients except Patients 25 and 27, who had mild weakness of distal leg muscles.

Seven patients (Patients 12–17, and 29) developed childhood sensory ataxia, moderate psychomotor delay, and cerebellar dysfunction, which were associated with retinal pigmental degeneration and heel cord tighten-

From the Departments of *Neurology and †Neuroradiology, National Neurological Institute "C Besta," Milan, Italy.

Received Jun 4, 1999, and in revised form Aug 5. Accepted for publication Aug 5, 1999.

Address correspondence to Dr Sghirlanzoni, Department of Neurology, National Neurological Institute "C Besta," Via Celoria 11, 20133 Milan, Italy.

ing in Patients 13 and 14. Four of them (Patients 12–15) had vitamin E deficiency (range, 0.15–0.44 mg%; normal values, 0.75–1.70 mg%). In Patients 16 and 17, spinocerebellar syndrome remained unclassified after metabolic disorders, spinocerebellar (SCA 1, 2, and 3), and Friedreich's ataxia were ruled out. Mitochondrial encephalomyopathy was diagnosed in Patient 29, although mutations for neuropathy, ataxia, and retinitis pigmentosa (NARP), mitochondrial encephalomyopathy with lactic acidosis and stroke-like episodes (MELAS), and myoclonus epilepsy with ragged-red fibers (MERRF) were not detected.

Laboratory Studies

Sjögren's syndrome and autoimmune active hepatitis were diagnosed in Patients 7 and 8, respectively. Anti-Hu antibodies were detected in Patients 9 and 10. Human immunodeficiency virus infection was found in Patient 11. Seven patients (Patients 18–24) had vitamin B_{12} deficiency (range, 25–154 pg/ml; normal values, 179–1,200 pg/ml), related to pernicious anemia (Patients 18, 20, and 23), strict vegetarian diet (Patient 21), and previous heavy alcohol intake (Patients 19, 22, and 24). Cerebrospinal fluid examination revealed mild protein increase (range, 53–92 mg%) in 9 patients.

Neurophysiological Findings

Sensory nerve action potential amplitudes were diffusely reduced or absent in 27 patients, consistent with axonal neuropathy. Mild decrease of compound motor action potential amplitudes in individual nerves of lower limbs and minimal chronic denervation on electromyogram were found in most cases. In all, follow-up showed unvaried changes, whereas in Patients 25 and 27, neuropathy became sensorimotor. Somatosensory evoked potential recording disclosed absent or markedly depressed amplitude of peripheral latencies with low amplitude and mild prolongation of scalp-recorded peaks (P37 and N20) in most patients. Delayed central sensory pathway conduction was clearly established in a few patients (Patients 4, 14, 15, 23, and 29).

MRI Findings

Cervical spine MRI scanning was performed 4.6 years (range, 0.6–25 years) after disease onset and disclosed axial T2-weighted high signal intensity in the posterior columns in 22 patients (Fig 1). T2 changes longitudinally extended at the dorsal medulla and at the thoracic and lumbar levels as well (Fig 2). In Patient 11, MRI scanning was normal, 5 weeks after onset of symptoms, but revealed clear abnormalities 4 years later. Follow-up MRI scanning was unvaried in 3 other patients (Patients 1, 2, and 8).

In 5 cases (Patients 25–29) and in sensorimotor axonal neuropathies, cervical MRI scanning was normal. In a similar manner, there were no posterior column abnormalities in 2 patients (Patients 23 and 24) with vitamin B_{12} deficiency, 3 and 10 months after cobalamin treatment was started.

Course and Treatment

All patients except Patient 11, who improved spontaneously 1 year after onset, showed a slow worsening of symptoms. Daily living activities were impaired in 4 patients (Patients 2–4, and 8), whereas 2 patients (Patients 10 and 13) became chairbound. Eight patients (Patients 2, 3, 5, 8–10, 25, and 27) received oral prednisone, immunosuppression (azathioprine or cyclophosphamide), or both, during the course of the disease, but treatment proved unsuccessful.[7,8] Tocopherol acetate (1,200 mg/day) was started in all patients with vitamin E deficiency and unequivocal improvement was observed only in Patient 14. Patients with vitamin B_{12} deficiency received cobalamin treatment until serum levels, mean corpuscular volume, and ataxia improved.

Discussion

Unlike peripheral motor disorders, sensory disturbances are less frequently diagnosed by the probable site of pathology. Primary ganglionopathies should be distinguished from sensory axonal neuropathies because of different pathogeneses and, therefore, a possibly different therapeutic approach. Ganglionopathies can occur as a paraneoplastic syndrome[9] and can be associated with dysimmune disorders,[7,10] acquired immunodeficiency syndrome,[11] drug and environmental intoxications,[12,13] vitamin E deficiency,[14] and spinocerebellar degeneration.[15] However, their cause often remains unsettled, although in idiopathic cases, an autoimmune attack to the DRG, possibly allowed by the lack of blood–brain barrier, was suggested.[8,10]

Primary loss of DRG neurons causes the degeneration of both peripheral and central sensory projections, with involvement of large-diameter sensory fibers and short-length axons, such as trigeminal and truncal nerves, in a fashion that is not length dependent.[7] This leads to early gait and limb ataxia, widespread deep tendon hyporeflexia, and asymmetric or patchy cutaneous sensory disturbances. As rarely seen in ganglionopathies, 3 of our patients (Patients 1, 2, and 5) had nystagmus, possibly related to proprioceptive vestibular dysfunction. Diagnosis may be easier in subacute settings,[16] after ataxic Guillain-Barré syndrome is ruled out. Conversely, in chronic ganglionopathies,[8,10] clinical features may overlap those of sensory axonal neuropathies. Evidence of central sensory pathway involvement could definitely localize the disease process to the DRG. However, potential electrodiagnostic findings are usually obscured by attenuated sensory nerve action potential amplitudes.

Table. Patient Data

	Sex	Age at Onset (yr)	Follow-Up (yr)	Ataxia	Sensory Loss	Positive Symptoms	Distribution of Sensory Dysfunction
Patient							
1	F	56	3	+	V, K > T-P	+	Stocking-glove
2	F	47	4	+	V, K > T-P	−	Stocking-glove
3	M	49	10	+	V, K	+	Stocking-glove
4	F	46	1	+	V, K	+	Patchy at trunk and limbs
5	M	48	9	+	V, K > T-P	+	Stocking-glove, later trunk asymmetrically
6	M	49	1	−	V, K > T-P	−	Patchy at upper limbs, left arm pseudoathetosis
7	F	67	4	+	V, K > T-P	+	Patchy at face and hands
8	M	43	1	+	V, K > T-P	+	Patchy at trunk and limbs
9	F	58	−	+	V, K > T-P	+	Stocking-glove, later trunk asymmetrically
10	M	58	−	+	V, K	+	Trunk D5–D10, limbs pseudoathetosis
11	M	37	4	+	V, K	+	Stocking-glove, UL pseudoathetosis
12	F	15	2	+	V, K	−	LL > UL
13	F	13	1	+	V, K	−	LL > UL
14	M	<10	16	+	V, K	−	Distal LL
15	M	<10	2	+	V, K	−	Distal LL
16	F	14	1	+	V, K	−	Distal LL
17	F	<10	1	+	V, K	+	Distal LL
18	M	75	1	+	V, K; T-P	+	Stocking-glove
19	M	40	2	+	V, K; T-P	+	Stocking-glove
20	F	68	1	+	V, K	+	Distal LL
21	M	46	1	−	−	+	Distal UL, thighs
22	M	50	1	+	V, K; T-P	−	Distal LL
23	M	61	1	+	V, K; T-P	+	Stocking-glove
24	F	51	1	+	V, K > T-P	+	Stocking-glove
25	M	75	1	+	T-P > V, K	+	Stocking-glove
26	M	37	0,5	+	T-P > V, K	+	Distal LL
27	M	57	6	+	T-P > V, K	−	Stocking-glove
28	F	68	0,5	−	−	+	Distal LL
29	M	<10	2	+	V, K	−	Distal LL

[a]Intraepidermal nerve fiber density at distal leg = 5.3/mm (normal values, 13.3 ± 6.5/mm), at proximal thigh = 25.2/mm (normal values, 24 ± 8.4/mm)[6]

[b]Complex II = 18.3 nmol/min/mg (normal values, 20–40 nmol/min/mg); complex III = 68 nmol/min/mg (normal values, 80–160 nmol/min/mg), on muscle biopsy.

V = vibratory; K = kinesthetic; T-P = light touch and pain; UL = upper limbs; LL = lower limbs; CSF = cerebrospinal fluid; SNAP = sensory nerve action potential; MRI = magnetic resonance imaging; HBc = hepatitis B core antibody; ANA = anti-nuclear antibody; ASMA = anti–smooth muscle antibody; RF = rheumatoid factor; APCA = anti–parietal cell antibody; MCV = mean corpuscular volume; MGUS = monoclonal gammopathy of undetermined significance; ND = not done.

Laboratory Findings	CSF	SNAP Amplitude	MRI	Diagnosis
−	−	All severely reduced	T2+	Idiopathic ganglionopathy
−	−	All severely reduced	T2+	Idiopathic ganglionopathy
−	Protein 92 mg%	Reduced legs > arms	T2+	Idiopathic ganglionopathy
ANA 1:160	−	All severely reduced	T2+	Idiopathic ganglionopathy
−	−	All severely reduced	T2+	Idiopathic ganglionopathy
−	−	Asymmetric reduction arms > legs	T2+	Idiopathic ganglionopathy
Schirmer's test +, lip biopsy +, anti-Ro +	ND	All reduced	T2+	Sjögren's syndrome–associated ganglionopathy
HBc, ANA, ASMA, RF +, hyperglobulinemia	−	All absent	T2+	Autoimmune hepatitis–associated ganglionopathy
Anti-Hu +	−	All severely reduced	T2+	Paraneoplastic ganglionopathy
Anti-Hu +	Protein 75 mg%	All absent	T2+	Paraneoplastic ganglionopathy
HIV infection	Protein 80 mg%	All severely reduced	T2+	AIDS-associated ganglionopathy
Vitamin E deficiency, reduced triglyceridemia and cholesterolemia	ND	All severely reduced	T2+	Vitamin E deficiency
Vitamin E deficiency, reduced pre-β-lipoprotein	ND	All severely reduced	T2+	Vitamin E deficiency
Vitamin E deficiency, reduced triglyceridemia and cholesterolemia	Protein 53 mg%	All severely reduced	T2+	Vitamin E deficiency
Vitamin E deficiency, reduced pre-β-lipoprotein	ND	All severely reduced	T2+	Vitamin E deficiency
−	Protein 53 mg%	Reduced legs > arms	T2+	Spinocerebellar ataxia
−	−	Reduced legs > arms	T2+	Spinocerebellar ataxia
Vitamin B_{12} deficiency, APCA +	ND	All reduced	T2+	Subacute combined degeneration
Vitamin B_{12} deficiency	−	Reduced legs > arms	T2+	Subacute combined degeneration
Vitamin B_{12} deficiency, APCA +	ND	Reduced in arms	T2+	Subacute combined degeneration
Vitamin B_{12} deficiency	ND	Normal	T2+	Subacute combined degeneration
Vitamin B_{12} deficiency	Protein 62 mg%	All reduced	T2+	Subacute combined degeneration
Vitamin B_{12} deficiency, APCA +	Protein 62 mg%	Reduced in legs	−	Subacute combined degeneration
Vitamin B_{12} deficiency	Protein 78 mg%	All severely reduced	−	Subacute combined degeneration
MCV 99.4 fl	ND	All severely reduced	−	Alcoholic neuropathy
MCV 100 fl	Protein 82 mg%	Reduced in legs	−	Alcoholic neuropathy
IgG-λ MGUS	−	All absent	−	MGUS-associated neuropathy
IgM-κ MGUS	ND	Normal	−	Small-fiber sensory neuropathy[a]
Decreased respiratory chain activity[b]	ND	All absent	−	Mitochondrial encephalomyopathy, sensory neuropathy

In the present series, 22 of 29 patients showed axial T2-weighted MRI high signal intensity in the posterior columns of the cervical spine, reflecting the degeneration of central sensory projections. Similar changes have been reported previously in a few patients with ganglionopathy[3–5] and were shown to correlate with pathological findings.[17] In Patients 1 through 11, T2 abnormalities correlated well with the clinical diagnosis of sensory ganglionopathy,[3] which included idiopathic,[8] paraneoplastic,[9] acquired immunodeficiency syndrome,[11] Sjögren's syndrome,[7] and autoimmune chronic active hepatitis-associated[18] cases. In particular, in all patients, gait

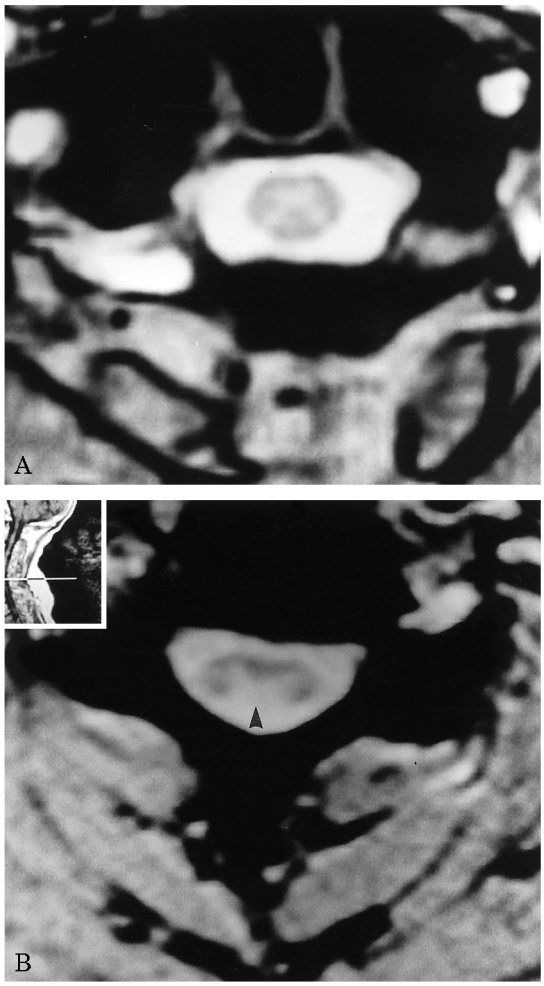

Fig 1. Axial T2-weighted gradient echo magnetic resonance imaging scans (repetition time, 500 msec; echo time, 9 msec; flip angle, 20°) of cervical spinal cord (C4 level) (A) Normal appearance of posterior column white matter and of anterior and posterior horns. (B) Arrow *shows diffuse high signal intensity in the posterior columns (Patient 1).*

ataxia was the presenting symptom, and in most of them, cutaneous sensory disturbances involved face, trunk, and limbs in a patchy fashion. Moreover, 5 patients (Patients 6–10) had autonomic dysfunction. Posterior column abnormalities that persisted after symptoms spontaneously improved (Patient 11) strengthened the correlation between clinical and MRI findings. T2 changes extending throughout the length of the posterior columns confirmed that patients did not have length-dependent fiber degeneration seen in "dying back" disorders, but had DRG degeneration (see Fig 2).

Control sensorimotor axonal neuropathies and Patients 25 through 29, whose clinical picture was consistent with length-dependent neuropathy, did not show abnormalities on MRI scanning, therefore providing specificity to T2 changes in primary ganglionopathies.

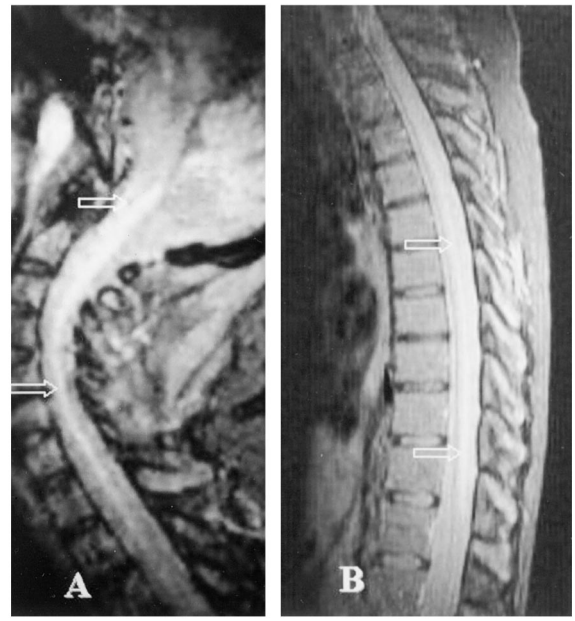

Fig 2. Sagittal T2-weighted gradient echo magnetic resonance imaging scans disclosed high signal intensity throughout the length of the posterior columns in Patient 1. Arrows *indicate T2 changes at the dorsal medulla and cervical spine (A) and at the thoracic and lumbar levels (B). Similar abnormalities were also found in Patient 3.*

DRG neurons are commonly affected in both vitamin E deficiency[14] and spinocerebellar ataxia.[15] In all our patients (Patients 12–17), MRI scanning consistently demonstrated T2 hyperintensity in the posterior columns.[19] Similar changes were found in all patients with vitamin B_{12} deficiency (Patients 18–22) before cobalamin replacement. Recovery of MRI changes after treatment is well known[20] and supports that myelin is primarily affected. However, electrodiagnostic evidence of axonal neuropathy in all our patients, which was surprisingly limited to the upper limbs in one case (Patient 20), suggested the involvement of DRG neurons.

In conclusion, T2-weighted MRI scanning provided evidence of central pathway impairment in chronic ataxic sensory neuropathies and localized the pathological process to the DRG.

References

1. Wokke JH, van Dijk GW. Sensory neuropathies including painful and toxic neuropathies. J Neurol 1997;244:209–221
2. Asbury AK, Brown MJ. Sensory neuronopathy and pure sensory neuropathy. Curr Opin Neurol Neurosurg 1990;3:708–711
3. Yasuda T, Sobue G, Mokuno K, et al. Clinico-pathological features of acute autonomic and sensory neuropathy: a long-term follow-up study. J Neurol 1995;242:623–628
4. Sobue G, Yasuda T, Kumazawa K, et al. MRI demonstrated

dorsal columns involvement of the spinal cord in Sjögren's syndrome-associated neuropathy. Neurology 1995;45:592–593
5. Waragai M, Tayaka Y, Hayashi M. Serial MR finding of chronic idiopathic ataxic neuropathy. J Neurol Sci 1997;151: 93–95
6. McArthur JC, Stocks AE, Hauer P, et al. Epidermal nerve fiber density: normative reference range and diagnostic efficiency. Arch Neurol 1998;55:1513–1520
7. Griffin JW, Cornblath DR, Alexander E, et al. Ataxic sensory neuropathy and dorsal root ganglionitis associated with Sjögren's syndrome. Ann Neurol 1990;27:304–315
8. Dalakas MC. Chronic idiopathic ataxic neuropathy. Ann Neurol 1986;19:545–554
9. Chalk CH, Windebank AJ, Kimmel DW, McManis PG. The distinctive clinical features of paraneoplastic sensory neuronopathy. Can J Neurol Sci 1992;19:346–351
10. Sobue G, Yasuda T, Kachi T, et al. Chronic progressive sensory ataxic neuropathy: clinicopathological features of idiopathic and Sjögren's syndrome-associated cases. J Neurol 1993;240:1–7
11. Scaravilli F, Sinclair E, Arango JC, et al. The pathology of the posterior root ganglia in AIDS and its relationship to the pallor of the gracile tract. Acta Neuropathol 1992;84:163–170
12. Schaumburg HH, Kaplan J, Windebank AJ, et al. Sensory neuropathy from pyridoxine abuse: a new megavitamin syndrome. N Engl J Med 1983;309:445–448
13. Schaumburg HH, Berger AR. Human toxic neuropathy due to industrial agents. In: Dyck PJ, Thomas PK, Griffin JW, et al, eds. Peripheral neuropathy. Philadelphia: WB Saunders, 1993: 1533–1548
14. Kayden HJ. The neurological syndrome of vitamin E deficiency: a significant cause of ataxia. Neurology 1993;43: 2167–2169
15. McLeod JG, Evans WA. Peripheral neuropathy in spinocerebellar degenerations. Muscle Nerve 1981;4:51–61
16. Windebank AJ, Blexrud MD, Dyck PJ, et al. The syndrome of acute sensory neuropathy: clinical features and electrophysiologic and pathologic changes. Neurology 1990;40:584–591
17. Okumura R, Asato R, Shimada T, et al. Degeneration of the posterior columns of the spinal cord: postmortem MRI and histopathology. J Comput Assist Tomogr 1992;16:865–867
18. Merchut MP, Adams EM, Morrissey MM. Sensory neuronopathy in autoimmune chronic active hepatitis. Neurology 1993; 43:2410–2411
19. Vorgerd M, Tegenthoff M, Kühne D, Malin JP. Spinal MRI in progressive myeloneuropathy associated with vitamin E deficiency. Neuroradiology 1996;38(Suppl 1):S111–S113
20. Hemmer B, Glocker FX, Schumacher M, et al. Subacute combined degeneration: clinical, electrophysiological, and magnetic resonance imaging findings. J Neurol Neurosurg Psychiatry 1998;65:822–827

Atypical Refsum Disease with Pipecolic Acidemia and Abnormal Catalase Distribution

M. R. Baumgartner, MD,*¶ G. A. Jansen, PhD,†
N. M. Verhoeven, PhD,‡ P. A. W. Mooyer, MSc,†
C. Jakobs, PhD,‡ F. Roels, MD,§ M. Espeel, PhD,§
A. Fourmaintraux, MD,‖ H. Bellet, PhD,¶
R. J. A. Wanders, PhD,† and J. M. Saudubray, MD*

We describe an 18-year-old patient with psychomotor retardation and abnormally short metatarsi and metacarpals but no other signs of classic Refsum disease. Molecular analysis of the phytanoyl–coenzyme A hydroxylase gene revealed a homozygous deletion causing a frameshift. Surprisingly, L-pipecolic acid was elevated in plasma, and microscopy of the liver showed a reduced number of peroxisomes per cell and a larger average peroxisome size. These abnormal peroxisomes lacked catalase as did peroxisomes in fibroblasts of this patient. Such generalized peroxisomal abnormalities are not present in classic Refsum disease.

Baumgartner MR, Jansen GA, Verhoeven NM, Mooyer PAW, Jakobs C, Roels F, Espeel M, Fourmaintraux A, Bellet H, Wanders RJA, Saudubray JM. Atypical Refsum disease with pipecolic acidemia and abnormal catalase distribution. Ann Neurol 2000;47:109–113

Refsum disease (RD) is an autosomal recessive disorder characterized by retinitis pigmentosa, peripheral neuropathy, cerebellar ataxia, and increased cerebrospinal fluid protein. Phytanoyl–coenzyme A (CoA) hydroxylase (*PhyH*), a peroxisomal matrix protein, is deficient, leading to accumulation of phytanic acid in tissues.[1,2] Other peroxisomal functions and structure are normal

From the *Department of Pediatrics, Hôpital Necker–Enfants Malades, Paris, and ¶Laboratoire de Biochimie Médicale B, Hôpital Saint-Eloi, Montpellier, France; †Department of Pediatrics and Clinical Chemistry, University Hospital Amsterdam, and ‡Department of Clinical Chemistry, Metabolic Unit, Free University Hospital, Amsterdam, The Netherlands; §Department of Human Anatomy, Embryology, and Histology, University of Ghent, Belgium; and ‖Department of Pediatrics, Centre Hospitalier Sud, Saint-Pierre, La Réunion.

Received Mar 15, 1999, and in revised form Jul 27. Accepted for publication Aug 6, 1999.

Address correspondence to Dr Saudubray, Department of Pediatrics, Hôpital Necker–Enfants Malades, 149 rue de Sèvres, 75743 Paris, Cedex 15, France.

¶Present address: Department of Pediatrics, Johns Hopkins University School of Medicine, PTCB 803, 725 North Wolfe Street, Baltimore, MD 21205.

in classic RD. Phytanic acid is an unusual branched-chain fatty acid (3,7,11,15-tetramethylhexadecanoic acid) originating exclusively from dietary sources which accumulates in a variety of inherited peroxisomal disorders, including classic RD, rhizomelic chondrodysplasia punctata, and other peroxisome biogenesis disorders.[2–5] Inactivating mutations in the *PhyH* gene have been identified in all patients with RD studied so far.[1,6–9]

L-Pipecolic acid is an intermediate in lysine catabolism, which is oxidized to α-aminoadipic acid by pipecolic acid oxidase, a peroxisomal matrix enzyme in human beings. Plasma L-pipecolic acid levels are increased 10 to 100 times in peroxisome biogenesis disorders of the Zellweger spectrum, whereas normal levels are found in RD, rhizomelic chondrodysplasia punctata, and isolated defects of peroxisomal β-oxidation.[4,5]

Here, we describe a unique patient presenting with an atypical form of RD characterized by deficient *PhyH*, elevated pipecolic acid, and abnormal catalase distribution in liver and fibroblasts.

Case Report

This female child of nonconsanguineous healthy parents living in La Réunion was born at term after an uneventful pregnancy. At 10 years of age, she entered a special school because of mild developmental delay. Cranial asymmetry, retrognathism, dental dysharmony, and distal osseous abnormalities were noted. Two years later, a random screening of plasma amino acids revealed elevated plasma pipecolic acid (113 mmol/L [control values < 2.5 mmol/L]), and she was referred to our metabolic unit. She was in excellent general health. Except for a systolic murmur, the results of her examination were normal. Evaluation of her psychomotor status showed mild developmental delay with language difficulties and partial alexia (determined by means of the Brunet-Lézine scale for psychomotor development in childhood). Echocardiography revealed a mitral prolapse with mild mitral insufficiency and minimal aortic insufficiency. Skeletal radiography showed short fourth and fifth metacarpals and short first metatarsi. There were no anomalies of long bones and no ectopic calcifications or osteoporosis. Cerebral magnetic resonance imaging, including regional cerebral blood flow, was normal as were an electroencephalogram, ophthalmological examination, electroretinogram, and visual evoked potentials. Abdominal ultrasound displayed small renal cysts at the poles of both kidneys. The liver was of normal size and structure. A liver biopsy showed predominantly microvesicular steatosis and periportal fibrosis. Repeat plasma amino acid determination confirmed an elevated pipecolic acid concentration.

At 18 years of age, the patient presents with retinitis pigmentosa and attends special school because of her mild psychomotor retardation. She has no evidence of cutaneous abnormalities, ataxia, peripheral neuropathy, or hearing loss.

Methods

Peroxisomal parameters were measured in plasma according to previously described methods.[5] Pipecolic acid was quantified with electron-capture detection after derivatization by capillary column gas chromatography.[10] Enantiomeric separation of D- and L-pipecolic acid was performed by analyzing the same derivative of pipecolic acid on a chiral capillary column (CP-Chirasil-Dex CB [25 × 0.25 mm, 0.25-mm film thickness]; Chrompack, Middleburg, The Netherlands), whereby detection was accomplished by mass fragmentography.

Peroxisomal functions, catalase immunofluorescence, and the immunoblotting procedure for acyl-CoA oxidase and 3-oxoacyl-CoA thiolase were determined in cultured fibroblasts as described.[5]

Liver peroxisomes were visualized for light and electron microscopy by staining for catalase activity and by protein A–colloid gold immunolocalization as previously described.[11]

Morphometry of proxisomes was performed on random electron micrographs with a semiautomated device.[12]

Complementation analysis using cultured skin fibroblasts and measurement of phytanic acid α-oxidation was performed as described.[13,14]

Reverse transcriptase polymerase chain reaction (RT-PCR) analysis of fibroblast *PhyH* messenger RNA was performed as described.[8] The mutation c.375delGG was confirmed by PCR amplification of the corresponding genomic fragment followed by sequence analysis.

Consent for all studies described was obtained from the patient's parents.

Results

Concentrations of phytanic and pipecolic acid were highly elevated in plasma (Table), whereas those of

Table. Biochemical Findings in Plasma and Cultured Skin Fibroblasts

Parameter	Index Patient	Control
Plasma		
Pipecolic acid (μmol/L)	62.1	0.54–2.46
Phytanic acid (μmol/L)	274	0.01–9.88
Pristanic acid (μmol/L)	1.01	0.01–2.98
Pristanic acid:phytanic acid ratio	0.004	0.05–0.40
Fibroblasts		
$C_{26:0}$ β-oxidation (pmol/hr/mg protein)	1,072	1,002 ± 336
Pristanic acid β-oxidation (pmol/hr/mg protein)	1,250	1,147 ± 325
Phytanic acid α-oxidation (pmol/hr/mg protein)	5.4	68 ± 13
Catalase immunofluorescence	Mosaic pattern	Particle bound

very long chain fatty acids (VLCFAs), pristanic acid, and bile acid intermediates were normal as were erythrocyte plasmalogen levels. The enantiomeric analyses of D- and L-pipecolic acid revealed that the configuration of plasma pipecolic acid was L, the biological form. The pristanic:phytanic acid ratio was low, suggesting an isolated deficiency of phytanic acid α-oxidation. This was demonstrated directly by measuring phytanic acid α-oxidation in cultured skin fibroblasts. The patient's value was 8% of that of a control with normal oxidation of VLCFAs (C26) and pristanic acid β-oxidation (see Table). Fibroblast VLCFA levels, de novo plasmalogen synthesis, and dihydroxyacetonephosphate acyltransferase activity were normal. Immunoblotting studies of extracts of cultured fibroblasts showed a normal amount of peroxisomal acyl-CoA-oxidase and 3-oxoacyl-CoA thiolase. Interestingly, catalase immunofluorescence in fibroblasts showed a mosaic pattern clearly different from that of a control (Fig 1). When 50 cells from the index patient were compared, 16 (32%) showed the punctate pattern found in control cells. Twenty cells (40%) displayed about half the amount of particle-bound catalase, and in 14 cells (28%), no particle-bound fluorescence was detected. By contrast, fibroblasts from classic RD patients all showed a punctate pattern (5 RD cell lines tested).

Light microscopy of the patient's liver showed a more severe defect, with virtually all cells showing cytoplasmic localization of catalase (Fig 2). In addition, the hepatocyte peroxisomes were unusually large, with membrane invaginations containing the three β-oxidation enzymes and alanine:glyoxylate aminotransferase antigens.[11] Catalase activity and antigen were negative or extremely weak in such organelles, indicating an isolated catalase import defect.[11] Morphometry confirmed the increased size (corrected mean diameter of circle = 0.907 mm [range in controls: 0.569–0.717 μm]; >95% percentile = 1.351 μm [controls: 0.768 μm]) and reduced number of peroxisomes (numerical density was 16% that of controls). Volume and surface density were reduced to 44% and 31%, respectively.

Complementation studies revealed that our patient belongs to the same complementation group as patients with classic RD, suggesting that the *PhyH* gene was the primary defect (data not shown).[8,9]

RT-PCR analysis of fibroblast *PhyH* messenger RNA revealed a 2–base pair deletion (approximately 375–376delGG), producing a frameshift at amino acid 127 (E127R) followed by a stop codon at amino acid 127 (D127X). Studies at the genomic level revealed that this mutation was homozygous. *PhyH* complementary DNA analysis of 29 classic RD patients showed no

Fig 1. Catalase immunofluorescence in cultured skin fibroblasts. All cells from a control individual (left panel) show a punctate pattern indicating normal import of catalase into peroxisomes. Cells from the index panel (right panel) show a mosaic distribution pattern: in some cells, the normal punctate pattern is found, whereas the amount of particle-bound catalase is decreased or even completely absent in other cells. This indicates an impaired import of catalase into peroxisomes of the index patient.

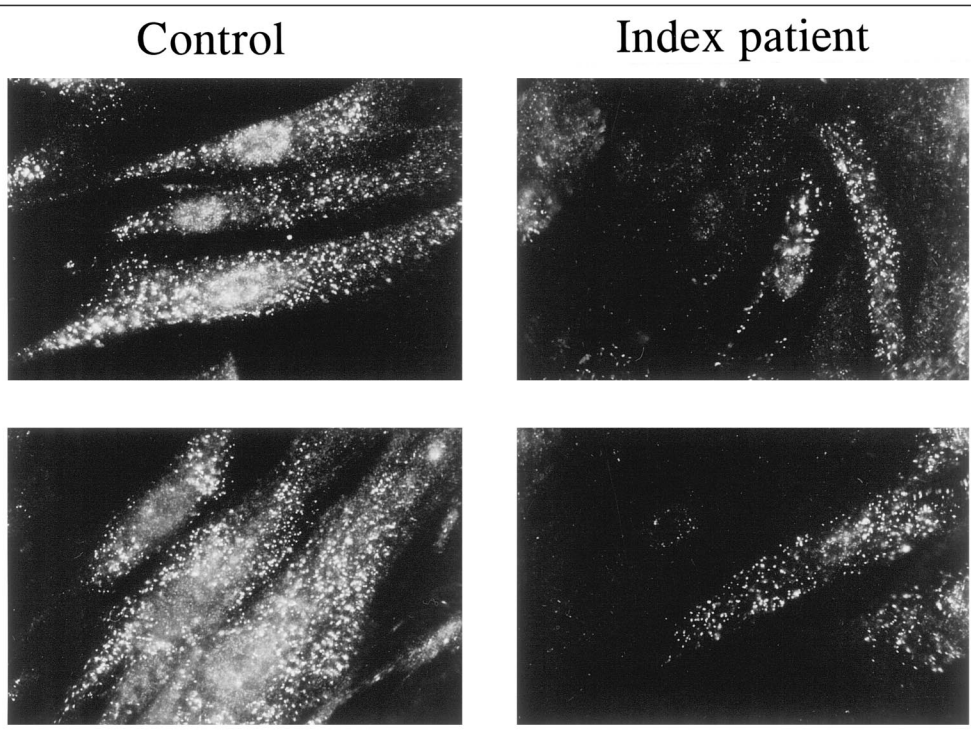

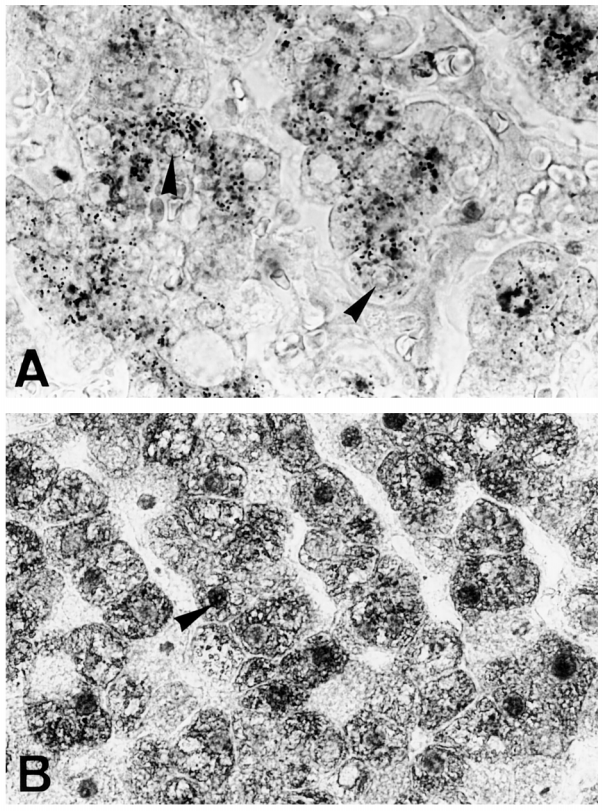

Fig 2. Catalase immunostaining in liver cryostat sections of a normal human control (A) and the patient (B). In the control, a granular reaction representing peroxisomal localization of catalase is seen in the parenchymal cells; the nuclei are unreactive (arrowheads). *In the patient, a diffuse cytoplasmic reaction delineating the cell borders is present, and many nuclei* (arrowhead) *also show immunoreactivity. (Magnification ×500).*

mutations in this region (G. A. Jansen and co-workers, unpublished results).

Discussion

Classic RD is characterized by retinitis pigmentosa, peripheral neuropathy, cerebellar ataxia, and elevated cerebrospinal fluid protein level. Most patients have clear-cut manifestations before the age of 20 years.[2] Several phenotypic variants of RD in which one or more of these abnormalities are not present have been described.[3,15] Our patient, now 18 years old, has retinitis pigmentosa but none of the other cardinal signs of RD. In addition, she has minor osseous abnormalities consistent with RD. Unlike classic RD patients, she has mild mental retardation and facial dysmorphism. The possibility that she will develop more typical signs of RD with time cannot be ruled out.

What is remarkably different from classic RD patients is the fact that our patient accumulated L-pipecolic acid and displayed abnormal hepatic and fibroblast peroxisomes with an abnormal catalase distribution, suggesting a more complex peroxisomal disorder. Pipecolic acid was normal in all 5 of our RD patients and in 10 RD patients at the Kennedy Krieger Institute (Ann Moser, personal communication, 1999). Tranchant and colleagues[16] described 4 related patients, of whom 3 had classic RD and the fourth died from a progressive neurological disorder with clinical and neuropathological abnormalities unusual for RD. Besides the phytanic acid oxidation defect, there was an increase in plasma pipecolic acid in 2 of these patients. Like our patient, all 4 patients had abnormal metatarsi, and 2 had severe psychomotor retardation. In the study by Tranchant and colleagues,[16] Case 1 resembles our patient in many aspects but showed cerebellar ataxia and peripheral neuropathy at the age of 30 years. Recent studies on fibroblasts from this family have shown that the deficiency of *PhyH* is caused by inactivating mutations in the hydroxylase gene.[17] In contrast to our patient, catalase immunofluorescence was normal in this family.[17]

Neither elevated L-pipecolic acid levels nor an abnormal subcellular distribution of catalase has ever been described in classic RD. These two phenotypic features cannot be ascribed to the presence of high levels of phytanic acid, because markedly elevated levels of this fatty acid are always present in classic RD. Thus, the underlying basis for the L-pipecolic acidemia and the abnormal subcellular distribution of catalase is uncertain. We cannot exclude the possibility that this patient has two or even three independent disorders, although the combination of three peroxisomal abnormalities would be extremely rare. The alternative possibility is that the truncated *PhyH* produced in this patient somehow has a secondary deleterious effect on peroxisomal function.

Our patient illustrates the importance of considering peroxisomal disorders in patients with mild mental retardation and bone abnormalities.

This study was supported by grants from the M. and W. Lichtenstein Stiftung and the Freiwillige Akademische Gesellschaft, Basel, Switzerland (Dr Baumgartner), and by the European Concerted Action "Peroxisomal Leukodystrophy" (BMH4, CT96-1621) and the Reserve Council of the University of Ghent (Dr Espeel).

References

1. Jansen GA, Wanders RJA, Watkins PA, Mihalik SJ. Phytanoyl-coenzyme A hydroxylase deficiency–the enzyme defect in Refsum's disease. N Engl J Med 1997;337:133–134
2. Steinberg D. Refsum disease. In: Scriver CR, Beaudet AL, Sly WS, Valle DE, eds. The metabolic and molecular basis of inherited disease. 7th ed. New York: McGraw-Hill, 1995:2351–2370
3. Skjeldal OH, Stokke O, Refsum S, et al. Clinical and biochemical heterogeneity in conditions with phytanic acid accumulation. J Neurol Sci 1987;77:87–96

4. Lazarow PB, Moser HW. Disorders of peroxisomal biogenesis. In: Scriver CR, Beaudet AL, Sly WS, Valle DE, eds. The metabolic and molecular basis of inherited disease. 7th ed. New York: McGraw-Hill, 1995:2287–2324
5. Baumgartner MR, Poll-The BT, Verhoeven NM, et al. Clinical approach to peroxisomal disorders. A series of 27 patients. Ann Neurol 1998;44:720–730
6. Jansen GA, Milhalik SJ, Watkins P, et al. Phytanoyl-CoA-hydroxylase is present in human liver, located in peroxisomes, and deficient in Zellweger syndrome: direct unequivocal evidence for the new, revised pathway of phytanic acid α-oxidation in humans. Biochim Biophys Res Commun 1996; 229:205–210
7. Jansen GA, Mihalik SJ, Watkins PA, et al. Phytanoyl-CoA hydroxylase is not only deficient in classical Refsum disease but also in rhizomelic chondrodysplasia punctata. J Inherit Metab Dis 1997;20:444–446
8. Jansen GA, Ofman R, Ferdinandusse S, et al. Refsum disease is caused by mutations in the phytanoyl-CoA hydroxylase gene. Nat Genet 1997;17:190–193
9. Mihalik SJ, Morrell JC, Kim D, et al. Identification of PAHX, a Refsum disease gene. Nat Genet 1997;17:185–189
10. Zee T, Stellard F, Jakobs C. Analysis of pipecolic acid in biological fluids using capillary gas chromatography with electron-capture detection and [$^2H_{11}$] pipecolic acid as internal standard. J Chromatogr 1992;574:335–339
11. Roels F, Espeel M, Poggi F, et al. Human liver pathology in peroxisomal diseases: a review including novel data. Biochimie 1993;75:281–292
12. Kerckaert I, de Craemer D, van Limbergen G. Practical guide for morphometry of human peroxisomes on electron micrographs. J Inherit Metab Dis 1995;18(suppl 1):172–180
13. Brul S, Westerfield A, Stijland A, et al. Genetic heterogeneity in the cerebrohepatorenal (Zellweger) syndrome and other inherited disorders with a generalized impairment of peroxisomal functions. J Clin Invest 1988;81:1710–1715
14. Wanders RJA, van Roermund CWT. Studies on phytanic acid α-oxidation in rat liver and cultured human skin fibroblasts. Biochim Biophys Acta 1993;1167:345–350
15. Poulos A, Pollard AC, Mitchell JC, et al. Patterns of Refsum's disease: phytanic oxidase deficiency. Arch Dis Child 1984;59: 222–229
16. Tranchant C, Aubourg P, Mohr M, et al. A new peroxisomal disease with impaired phytanic and pipecolic acid oxidation. Neurology 1993;43:2044–2048
17. Jansen GA, Ferdinandusse S, Verhoeven NM, et al. The classical Refsum disease gene (phytanoyl-CoA hydroxylase) is mutated in combined phytanic/pipecolic acidemia. J Inherit Metab Dis 1998;21(Suppl 2):109 (Abstract)

Diffusion-Weighted Magnetic Resonance Imaging in Boys with Neural Cell Adhesion Molecule L1 Mutations and Congenital Hydrocephalus

William D. Graf, MD,* Donald E. Born, MD, PhD,† Dennis W. W. Shaw, MD,‡ John R. Thomas, MD,§ Lynda W. Holloway, BS,‖ and Ron C. Michaelis, PhD‖

The phenotype of severe congenital hydrocephalus secondary to neural cell adhesion molecule L1 (L1CAM) gene mutations includes the distinct finding of brainstem corticospinal tract hypoplasia. Using diffusion-weighted imaging (DWI), we failed to demonstrate anisotropy in the corticospinal tracts of the basis pontis in 4 affected boys with L1CAM mutations. The DWI findings correlated with the neuropathological findings in a fifth patient. DWI may be a useful technique to screen for boys with L1CAM mutations.

Graf WD, Born DE, Shaw DWW, Thomas JR, Holloway LW, Michaelis RC. Diffusion-weighted magnetic resonance imaging in boys with neural cell adhesion molecule L1 mutations and congenital hydrocephalus. Ann Neurol 2000;47:113–117

X-linked hydrocephalus (XLH; MIM 307000) is associated with mutations of the neural cell adhesion molecule L1 (L1CAM), a 200-kd cell surface glycoprotein that is essential during early development for cell-to-cell adhesion, myelination, axonal guidance, and the process of fasciculation.[1–3] The most notable consequence of L1 protein disruption is the loss of corticospinal axon projections into the spinal cord.[2,4] XLH is the most severe phenotype within the spectrum of L1CAM disorders and is associated with the distinct neuropathological finding of corticospinal tract hypoplasia with absent medullary pyramids.[5,6] Milder L1CAM phenotypes include MASA syndrome (MIM

From the Departments of *Pediatrics and Neurology, †Pathology (Neuropathology), ‡Radiology, and §Anesthesiology, University of Washington School of Medicine, Seattle, WA; and ‖J. C. Self Research Institute, Greenwood Genetic Center, Greenwood, SC

Received Jun 23, 1999 and in revised form Aug 10. Accepted for publication Aug 10, 1999.

Address correspondence to Dr Graf, Division of Genetics and Development, Children's Hospital and Regional Medical Center, Mail Stop CH-47, 4800 Sand Point Way NE, Seattle, WA 98105.

303350), spastic paraplegia type I (MIM 312900), and agenesis of the corpus callosum.[7,8] Intrafamilial phenotypic heterogeneity is reported.[7–9] XLH is usually associated with those L1CAM mutations that produce truncation or gross rearrangements of the L1CAM protein.[7–11] Even if a patient falls within the L1CAM clinical spectrum, molecular genetic testing may be difficult to justify because of the expense and technical challenges of finding a mutation within the 29 exons of the large L1CAM gene.[11,12]

There is a need for further clinical, neuroradiological, neuropathological, and molecular genetic correlation studies to better define the L1CAM genotype-phenotype spectrum. Diffusion-weighted (magnetic resonance) imaging (DWI) has been used to detect the anisotropy of specific white matter tracts, including the corticospinal tract, and is able to show the structural degradation associated with Wallerian degeneration.[13–15] We hypothesized that DWI would not show the anisotropy in brainstem corticospinal tracts in L1CAM patients. We describe DWI findings in 4 boys with XLH and L1CAM mutations and the correlative neuropathology in a fifth affected boy.

Methods

Patients

The 5 patients were followed in the Birth Defects Clinic at Children's Hospital and Regional Medical Center (Seattle, WA). All 5 boys had a prenatal ultrasound diagnosis of hydrocephalus, planned Cesarean section deliveries, severe hydrocephalus at birth with occipital-frontal circumferences between 45 and 47 cm, and a thin rim of cerebral mantel of 1.5 cm or less on initial imaging studies. In all patients, a ventriculoperitoneal shunt was placed shortly after birth, and later imaging studies showed expansion of the brain parenchyma, agenesis of the corpus callosum, diffuse cerebral dysplasia, decreased white matter, and a small posterior fossa with the Chiari I malformation. All 5 boys had severe developmental disabilities: none could ambulate, transfer independently, or communicate verbally. Patients 1 and 5 had seizures that were difficult to control. Prior to L1CAM mutation analysis, informed consent was obtained from the parents of all subjects. The study was approved by the Institutional Review Committee of Self Memorial Hospital (Greenwood, SC).

Patient 5 died at the age of 12 years after a prolonged seizure. DNA was banked prior to death and later sent for L1CAM gene analysis. Consent was obtained for the performance of an autopsy. We have described his neuropathology prior to ascertainment of the L1CAM mutation.[6] The major neuropathological findings included dolichocephaly, diffuse polymicrogyria, pachygyria, leptogyria, and marked hypoplasia of the cerebral white matter. The ventricular cavities had fused ependyma-lined walls surrounded by gliotic tissue. Microscopically, there were six cortical layers with sparse cells and poorly organized lamination. The small hippocampi had sparse neurons, but the dentate gyrus was formed. The distal aqueduct was narrowed, and the fourth ventricle was not dilated. There were small cerebral peduncles and complete absence of the medullary pyramids.

Family Histories

Patients 1, 2, 3, and 4 had no family history of hydrocephalus or other developmental disabilities. Patients 1 and 2 are brothers with no other siblings. Patient 3 has 3 healthy older siblings. Patient 4 is an only child. Patient 5 had an older brother who died shortly after birth because of severe congenital hydrocephalus. His older sister is healthy, his mother's 2 brothers are normal, and his mother's sister had two miscarriages and 2 healthy daughters.

Genetic Analysis

The L1CAM mutations present in our patients were detected using restriction endonuclease fingerprinting protocols as described previously.[16]

DWI

MRI was performed on a General Electric Horizon LX 1.5-T system (General Electric Medical Systems, Milwaukee, WI). As a part of the clinical evaluation, routine sagittal and axial T1-weighted and axial fast-spin echo T2-weighted and FLAIR images of the entire brain were obtained. In addition, DWI was performed using a standard single-shot sequence. Parameters for the DWI were as follows: repetition time = 5,999, echo time = 99.1 FE, B = 1,000 sec/mm^2, field of view = 26 cm, slice thickness = 7.0 mm with 0.0 spacing, one excitation, and a 128 $\times$ 128 matrix. The scan time was 24 seconds. Anisotropy was evaluated by reviewing the component images in which diffusion gradients were employed in the *x*, *y*, and *z* directions (designated R/L [right-left], A/P [anterior-posterior], and S/I [superior-inferior] on the image annotation). Because of the pronounced susceptibility artifact in the caudal-most aspect of the posterior fossa, anisotropy was evaluated at the midpontine level. Midpontine DWI was visually analyzed to evaluate for the presence of the signal pattern that correlates to descending corticospinal tract anisotropy. For comparison, an adult patient with acute stroke was assessed using the identical DWI protocol.

Neuropathology

The brain of Patient 5 was removed within 48 hours after death, fixed in 10% buffered formalin for 10 days to 3 weeks, sectioned, and embedded in paraffin. Histological examination was performed on sections stained with hematoxylin-eosin and Luxol–fast blue/periodic acid–Schiff/hematoxylin. Luxol–fast blue stains were analyzed for distribution of myelinated white matter tracts.

Results

Genetic Analysis

We identified three novel L1CAM mutations: a 14–base pair deletion in exon 11 (nt 1340–1353) of Patients 1 and 2, a 1–base pair deletion in exon 10 (nt 1224) of Patient 3, and a point mutation at C466G in exon 5 of Patient 5 (Table). Mutations in these patients truncate the L1 protein in the extracellular domain and are expected to abolish cell surface expression

Table. L1CAM Gene Mutation, MRI, and Pontine DWI Findings in Patients with Severe Congenital Hydrocephalus, Flexion-Adduction Thumb Deformities, and Developmental Disabilities

Patient No.	Age (yr)	Postshunt MRI	Mutation Site (cDNA)	Mutation Site (AA)	Longitudinal Tract Anisotropy	Crossing Tract Anisotropy
1	7.0	ACC, DB, ↓WM, ChI	14-bp del exon 11 (nt 1340–1353)	FS 443 (+42)	Absent	Present
2	5.5	ACC, DB, ↓WM, ChI	14-bp del exon 11 (nt 1340–1353)	FS 443 (+42)	Absent	Present
3	1.3	ACC, DB, ↓WM, ChI	1-bp del exon 10 (nt 1224)	FS 407 (+28)	Absent	Present
4	3.5	ACC, DB, ↓WM, ChI	C550T	R184W	Absent	Present
5	12.0	ACC, DB, ↓WM, ChI	C466G exon 5	S156X	ND	ND

L1CAM = (neural) cell adhesion molecule L1; MRI = magnetic resonance imaging; DWI = diffusion-weighted imaging; cDNA = complementary DNA; AA = amino acid sequence; ACC = agenesis of the corpus callosum; bp = base pair; ChI = Chiari I malformation; del = deletion; DB = dysmorphic brain; FS x (+y) = frameshift after codon x plus y aberrant amino acids before a stop codon; ND = not determined; nt = nucleotide; ↓WM = paucity of white matter.

of the protein. The mutation at the amino acid site R184W in Patient 4 is a missense mutation that has been reported previously.[9] This mutation is expected to disrupt confirmation of the second immunoglobulin domain of the L1 protein.[17]

DWI

In the R/L diffusion gradient, the hypointense DWI signal that correlates to anisotropy in the crossing fiber tracts was present in Patients 1 through 4 (see Table; Fig 1). For the longitudinal fibers of the corticospinal tract, the expected hypointense DWI signal of the S/I diffusion gradient and the hyperintense DWI signal of the R/L diffusion gradient were not present in Patients 1 through 4. Figure 1 shows the findings in Patient 2 and an adult stroke patient tested for comparison.

Neuropathological Findings of the Pons

In Patient 5, the basis pontis was smaller than that of the adult stroke patient tested for comparison (Fig 2A

Fig 1. Axial T2-weighted (T-2) MRI (A), diffusion-weighted imaging (DWI) with right/left (R/L) diffusion gradient (B), and DWI with superior/inferior (S/I) diffusion gradient (C) of the midpons in an adult patient tested for comparison, who was evaluated after an acute cerebral infarct. Identical sequences (T2-weighted MRI [D], DWI with R/L gradient [E], and DWI with S/I gradient [F]) in Patient 2 show a smaller pons. The basilar artery (arrowhead) *and crossing fiber tracts* (straight arrow) *are identified in both subjects. Two foci* (*hyperintense with R/L gradient, hypointense with S/I gradient;* curved arrow) *consistent with the corticospinal tracts are seen anterior to the transverse fiber tracts in the normal pons (B and C) but not in the patient with X-linked hydrocephalus (E and F).*

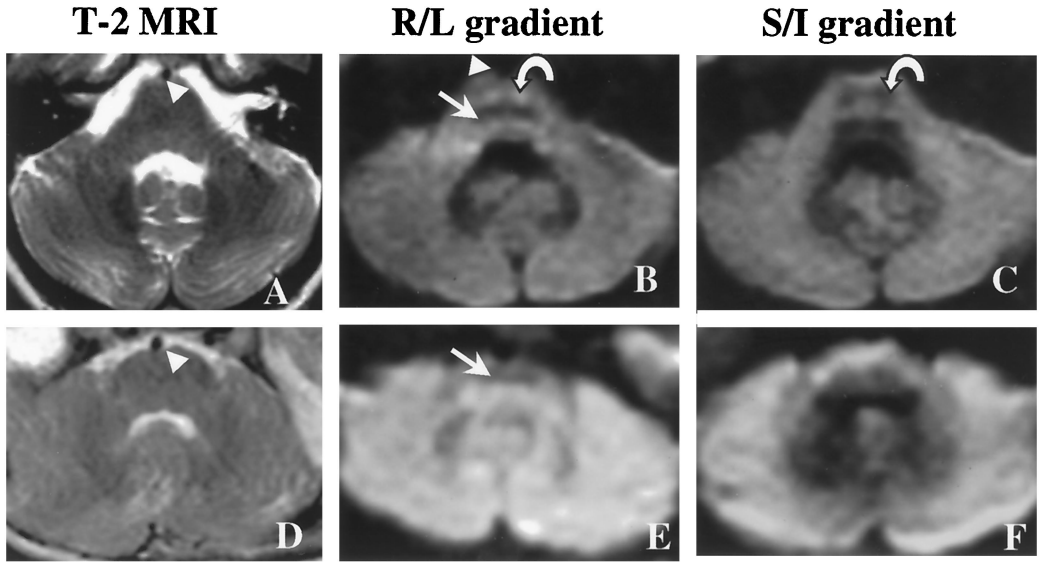

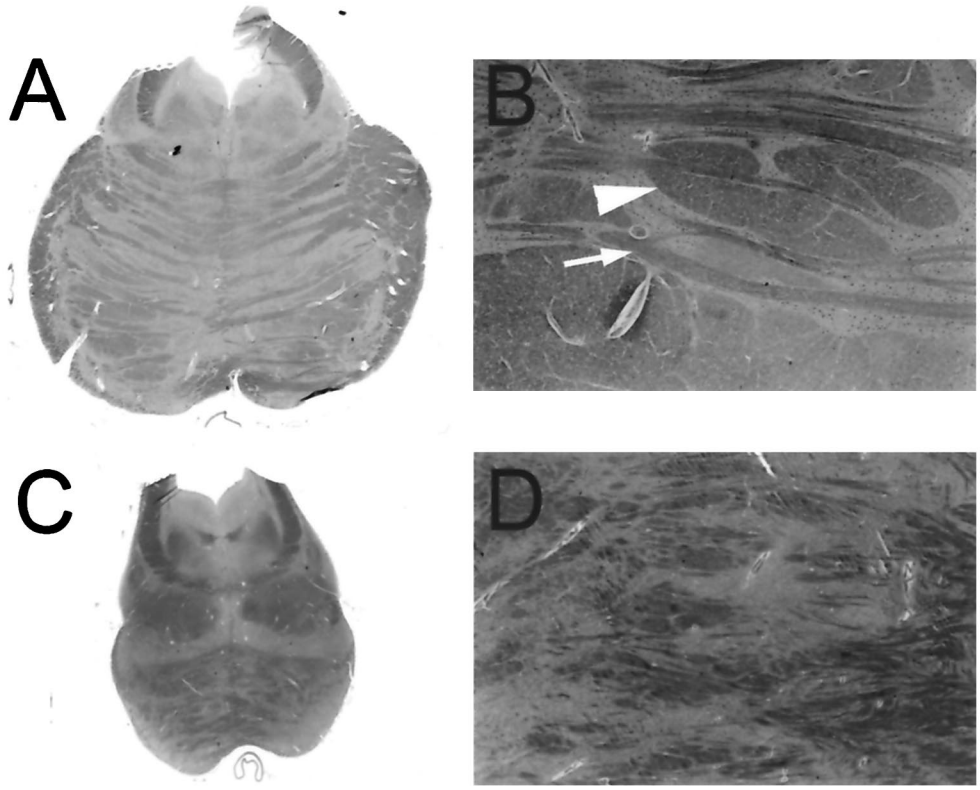

Fig 2. Transverse section of the pons from an adult control tested for comparison shows normal crossing and longitudinal fiber tracts (A and B). At low power (A), the basis pontis comprises two-thirds and the tegmentum comprises one-third of the transverse section. The medium power view (B) shows elongated fascicles that correspond to crossing tracts (arrow) *and rounded profiles* (arrowhead) *that correspond to longitudinal tracts. A transverse section of the pons (C) from Patient 5 demonstrates a smaller disproportionate pons (approximately one-third basis pontis and two-thirds tegmentum). Longitudinal corticospinal fiber tracts are not seen at medium power (D).*

and C). In the pons stained with Luxol-fast blue, crossing fiber tracts that correspond to cerebellopontine tracts were easily identified in both the control and Patient 5 (see Fig 2B and D). In contrast, longitudinal fiber tracts could not be identified in Patient 5 in the regions expected for corticospinal tracts (see Fig 2D).

Discussion

The identification of molecular errors that result in abnormal axonal growth and guidance is of increasing importance to both developmental neurobiologists and clinical neurologists.[1] This descriptive preliminary study supports the premise that DWI can show the absence of corticospinal axons in the brainstem of boys with L1CAM disorders. Although we could not adequately visualize the corticospinal tract at the level of the medullary pyramids, we were able to detect evidence of corticospinal tract hypoplasia at the level of the pons. This finding has not been emphasized in previous neuropathological studies of boys with XLH. DWI may provide a clinical screening tool prior to initiating a lengthy and laborious gene mutation analysis.

DWI can measure anisotropic diffusion of water molecules in white matter tracts.[15] This diffusion is restricted by macromolecules and membranes more in the transverse than in the longitudinal direction of the tracts. Because diffusion is measured independently in each direction, DWI provides a method of image contrast that is particularly suited to the study of fiber tracts or fascicles.[13,14]

Our study is the first attempt to image the brainstem in boys with XLH. There are some technological limitations to our study. The nontensor DWI used in this study does not provide quantitative measurements and can lead to underestimation of anisotropy. In addition, microscopic anisotropy can be masked by macroscopic isotropy if there is significant variability of brainstem fiber tract orientation within the voxel. More elaborate DWI examinations such as quantitative diffusion tensor MRI would provide more sensitive measures of anisotropy in these tracts.[13,18,19]

In conclusion, DWI may be a valuable technique in the identification of boys with XLH and potentially milder L1CAM phenotypes. Further studies are needed

to compare boys with L1CAM-defined XLH with children with non-L1CAM congenital hydrocephalus[5] and to assess the sensitivity and reliability of this technique within the L1CAM spectrum, ideally with more sophisticated DWI technology to obtain improved anatomical contrast.

References

1. Brümmendorf T, Kenwrick S, Rathjen FG. Neural cell recognition molecule L1: from cell biology to human hereditary brain malformations. Curr Biol 1998;8:87–97
2. Burden-Gulley SM, Pendergast M, Lemmon V. The role of cell adhesion molecule L1 in axonal extension, growth cone motility, and signal transduction. Cell Tissue Res 1997;290:415–422
3. Wood PM, Schachner M, Bunge RP. Inhibition of Schwann cell myelination in vitro by antibody to the L1 adhesion molecule. J Neurosci 1990;10:3635–3645
4. Cohen NR, Taylor JSH, Scott LB, et al. Errors in corticospinal axon guidance in mice lacking the neural cell adhesion molecule L1. Curr Biol 1997;8:26–33
5. Chow CW, Halliday JL, Anderson RM, et al. Congenital absence of pyramids and its significance in genetic diseases. Acta Neuropathol (Berl) 1985;65:313–317
6. Graf WD, Born DE, Sarnat HB. The pachygyria-polymicrogyria spectrum of cortical dysplasia in X-linked hydrocephalus. Eur J Pediatr Surg 1998;8 (Suppl I):10–14
7. Kenwrick S, Jouet M, Donnai D. X-linked hydrocephalus and MASA syndrome. J Med Genet 1996;33:59–65
8. Ruiz JC, Cuppens H, Legius E, et al. Mutations in L1CAM in two families with X linked complicated spastic paraplegia, MASA syndrome, and HSAS. J Med Genet 1995;32:549–552
9. Fransen E, Vits L, Coucke P, et al. The clinical spectrum of mutations in L1, neuronal cell adhesion molecule. Am J Med Genet 1996;64:73–77
10. Yamasaki M, Thompson P, Lemmon V. CRASH syndrome: mutations in L1CAM correlate with severity of the disease. Neuropediatrics 1997;28:175–178
11. Michaelis RC, Du YZ, Schwartz CE. The site of a missense mutation in the extracellular Ig of FN domains of L1CAM influences infant mortality and the severity of X linked hydrocephalus. J Med Genet 1998;35:901–904
12. Fransen E, Van Camp G, Vits L, Willems PJ. L1-associated diseases: clinical geneticists divide, molecular geneticists unite. Hum Mol Genet 1997;6:1625–1632
13. Nakada T, Nakayama N, Fujii Y, Kwee IL. Clinical application of three-dimensional anisotropy contrast magnetic resonance axonography. J Neurosurg 1999;90:791–795
14. Inoue T, Shimizu H, Yoshimoto T. Imaging the pyramidal tract in patients with brain tumors. Clin Neurol Neurosurg 1999;101:4–10
15. Makris N, Worth AJ, Sorensen AG, et al. Morphometry of in vivo human white matter association pathways with diffusion-weighted magnetic resonance imaging. Ann Neurol 1997;42: 951–962
16. Du YZ, Srivastava AK, Schwartz CE. Multiple exon screening using restriction endonuclease fingerprinting (REF): detection of six novel mutations in the L1 cell adhesion molecule (L1CAM) gene. Hum Mutat 1998;11:222–230
17. Bateman A, Jouet M, MacFarlane J, et al. Outline structure of the human L1 cell adhesion molecule and the sites where mutations cause neurological disorders. EMBO J 1996;15:6050–6059
18. Basser PJ, Mattiello J, LeBihan D. MR diffusion tensor spectroscopy and imaging. Biophys J 1994;66:259–267
19. Basser PJ, Pierpaoli C. A simplified method to measure the diffusion tensor from seven MR images. Magn Reson Med 1998; 39:928–934

A Nonsense Mutation of the *ATRX* Gene Causing Mild Mental Retardation and Epilepsy

Renzo Guerrini, MD,*† Jennifer L. Shanahan, MSc,‡ Romeo Carrozzo, MD,§ Paolo Bonanni, MD,* Douglas R. Higgs, MD,‖ and Richard J. Gibbons, MD‡

Mutations in the X-encoded gene *ATRX* are known to give rise to profound syndromal mental retardation (MR). Here, we describe a pedigree, including 4 affected family members with a 324C→T nonsense mutation in the *ATRX* gene. Although 2 patients have moderate to profound MR and the typical facial features of ATR-X syndrome, the other 2 patients presented with mild MR and epilepsy but without the characteristic facial dysmorphism. Mutations in the *ATRX* gene should be considered as a cause of mild MR in male patients lacking specific diagnostic features.

Guerrini R, Shanahan JL, Carrozzo R, Bonanni P, Higgs DR, Gibbons RJ. A nonsense mutation of the *ATRX* gene causing mild mental retardation and epilepsy. Ann Neurol 2000;47:117–121

Mental retardation affects approximately 3% of the population. To date, most advances have been made in the clinical and molecular diagnosis of profound (IQ < 20), severe (IQ 20–34), and moderate (IQ 35–50) mental retardation,[1] particularly those cases that are associated with characteristic clinical features (so-called syndromal mental retardation). Less progress has

From the *Institute of Child Neurology and Psychiatry, University of Pisa and Institute for Clinical Research, Stella Maris Foundation, Pisa, and §Servizio di Genetica Medica e Laboratorio di Citogenetica, Ospedale San Raffaele, Milano, Italy; †Division of Neurology, King's College, University of London, London, and ‡Nuffield Department of Clinical Biochemistry and Cellular Science, University of Oxford and ‖MRC Molecular Haematology Unit, Institute of Molecular Medicine, John Radcliffe Hospital, Oxford, UK.

Received Apr 23, 1999, and in revised form Aug 9. Accepted for publication Aug 10, 1999.

Address correspondence to Dr Gibbons, Nuffield Department of Clinical Biochemistry and Cellular Science, University of Oxford, John Radcliffe Hospital, Headington, Oxford, OX3 9DU, UK.

been made in understanding the causes of mild mental retardation (IQ 50–69), which is much more common and is frequently associated with a nonspecific phenotype providing no clues to help in the search for a genetic cause.

Mental retardation surveys show a substantial excess of affected male patients, and mutations in X-encoded genes may account for up to 25% of all cases.[2] To date, 25 genes are known to be involved in X-linked mental retardation, and most associated with syndromal mental retardation.[3] We now know that mutations in FMR1, which cause fragile X syndrome, give rise to a wide spectrum of disorders ranging from the classic syndrome to mild nonspecific mental retardation.[4]

We have previously identified a disease gene, *ATRX* in Xq13, which causes profound syndromal mental retardation (α thalassemia mental retardation) when mutated.[5] The ATR-X syndrome is characterized by profound mental retardation, a recognizable facial appearance, genital abnormalities, and an unusual form of α thalassemia; in addition, about one-third of patients have epilepsy.[6]

Prior to the identification of the *ATRX* gene, affected individuals could only be recognized on the basis of specific clinical and hematological criteria. Recent observations suggest that mutations in this gene cause a much broader phenotypic spectrum[7]; however, to date, all reported patients with *ATRX* mutations have presented with profound mental retardation.

Here, we report a novel *ATRX* mutation in a large family with 4 affected individuals with phenotypes ranging from many features of ATR-X syndrome (1 patient) to mild mental retardation, epilepsy, and only subtle dysmorphic features in whom the diagnosis of ATR-X syndrome would not have been considered in the absence of a family history.

Patients and Methods

The proband (Patient III-1), a mentally retarded child aged 13 years, presented with generalized convulsive seizures, facial features typical of ATR-X syndrome, and a family history of mental retardation and seizures. The extended pedigree, including 50 individuals from five generations, was investigated (Fig 1). All family members reside in Italy.

The 4 family members with mental retardation were submitted to cognitive testing using the Weschler intelligence scales.[8,9] Their adaptive level was determined by interviewing the parents using the Vineland Adaptive Behaviour Scales (VABS).[10] We classified mental retardation as mild, moderate, severe, and profound according to standard criteria.[1] Bone radiography, heart and abdominal ultrasonography, brain magnetic resonance imaging, and electroencephalographic investigations were performed.

Epstein-Barr virus–transformed lymphoblastoid patient cell lines were used as a source of DNA, RNA, and complementary DNA, which served as a template for mutation analysis. Mutations were characterized by ribonuclease cleavage and DNA sequencing as previously described (primer details available on request).[11]

The mutation creates an NpaIII restriction endonuclease site. Twenty-three family members were analyzed (4 affected male patients and 19 female family members) by amplification of DNA fragments containing the mutated site and digestion with NpaIII.

Results

The 4 affected patients showed a wide range of IQs and age-equivalent scores (Table). Patient III-10 had profound mental retardation, language limited to 10 words, and was entirely dependent on others for all daily activities. Patient III-1 had moderate mental deficits, poor language skills, and limited independence. Patients II-16 and II-18 had mild mental retardation with adequate language skills, held unskilled jobs, and led partially independent lives.

Generalized convulsive seizures were observed in 3 patients (Patients III-1, II-16, and II-18) during infancy and childhood but had been well controlled by anti-epileptic drugs; only Patient III-1 was still under treatment because of sporadic seizures. In Patients II-16 and II-18, seizures were the presenting symptom

Fig 1. Pedigree for family; the filled squares indicate affected male family members. Patient III-9 died at the age of 1 year from complications of general anesthesia.

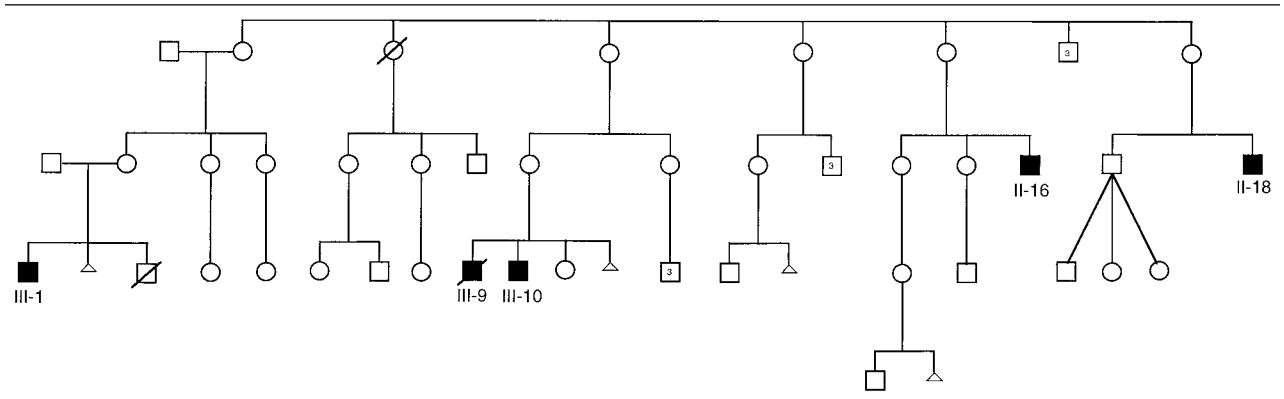

Table. Comparison of Clinical Features Between Previous Cases (total = 115) and the Family Reported Here

Clinical Features	Total[a]	%	Patient No. II-16 (45 yr)	II-18 (32 yr)	III-1 (17 yr)	III-10 (29 yr)
Profound mental retardation	114/114[b]	100	−	−	−	+
Weschler IQ scores						
FSIQ/verbal/performance			58[c]/62/57	56[c]/64/51	41[d]/45/49	N/A
VABS age equivalents						
Communication			7.3	7.5	3.2	1.8
Daily living skills			7.2	13	4.9	2.6
Socialization			7.2	7.4	3.1	1.5
Motor skills			3.8	5.9	5.0	2.5
Skeletal abnormalities	88/96	92	+[e]	+[f]	+[g]	+[h]
Characteristic face	90/99	91	−	−	+	+
Hemoglobin H inclusions	86/96	90	−	+	+	−
Neonatal hypotonia	63/71	89	−	−	+	+
Genital abnormalities	87/99	88	+[i]	−	−	−
Gut dysmotility	70/90	78	−	−	−	−
Microcephaly	69/93	74	−	−	+	−
Short stature	53/79	67	−	−	+	−
Seizures	36/105	34	+	+	+	−
Cardiac defects	20/103	19	−	−	−	−
Renal/urinary abnormalities	18/102	18	−	−	−	−

[a]Total represents number of patients on whom appropriate information is available and includes patients who do not have α thalassaemia but in whom *ATRX* mutations have been identified.
[b]1 patient too young (<1 year) to assess degree of mental retardation.
[c]Weschler Adult Intelligence Scale.
[d]Weschler Intelligence Scale for Children–revised.
[e]Camptodactyly.
[f]Drumstick distal phalanges.
[g]Delayed bone age, brachydactyly, camptodactyly.
[h]Kyphosis.
[i]Cryptorchidism.

FSIQ = full-scale intelligence quotient; N/A = too severely retarded for testing with Weschler scales; VABS = Vineland Adaptive Behaviour Scale.

at the ages of 1 and 3 years, respectively, after apparently normal early development. In those individuals with seizures, electroencephalographic investigations showed mild diffuse epileptiform abnormalities during childhood and adolescence; however, findings became normal in the 2 patients who had reached adulthood.

Brain magnetic resonance imaging was normal in all 4 patients. Other clinical features showed marked variability, ranging from those of Patient III-1 (with many features of ATR-X syndrome) to those of other patients with minor physical abnormalities detected only after comprehensive clinical and radiographic investigations (see Table; Fig 2).

Hematological indices of all 4 patients fell within the normal ranges for their age and sex. Hemoglobin H (HbH) inclusions were seen in 2 patients (0.006% red blood cells in Patient III-1, 0.003% red blood cells in Patient II-18); although inclusions were rare, the presence of any is indicative of α thalassemia. Analysis of the ζ- and α-globin genes appeared normal (data not shown), ruling out the inheritance of any of the common deletional forms of α thalassemia present in the Mediterranean population.

The complete coding region of the *ATRX* gene was analyzed and revealed a single base substitution in exon 2 giving rise to a premature in-frame stop codon (324C→T, Arg37Stop), which is the most 5′ mutation so far described. It lies in a highly conserved region of the ATRX protein. It creates an NpaIII restriction enzyme site, which was exploited to show that all 4 affected male and 10 female family members had the 324C→T mutation.

Alternative splicing leading to skipping of a mutation is a recognized cause of phenotypic rescue.[12] To determine whether the milder phenotype detected in some members of the family is associated with exon skipping, we analyzed RNA splicing around the exons closest to the mutation. Amplification of complementary DNA using different combinations of primers in the first five exons revealed no evidence of variation in messenger RNA splicing in affected individuals (data not shown).

Discussion

The *ATRX* gene was originally identified by positional cloning, using strictly defined diagnostic criteria, in-

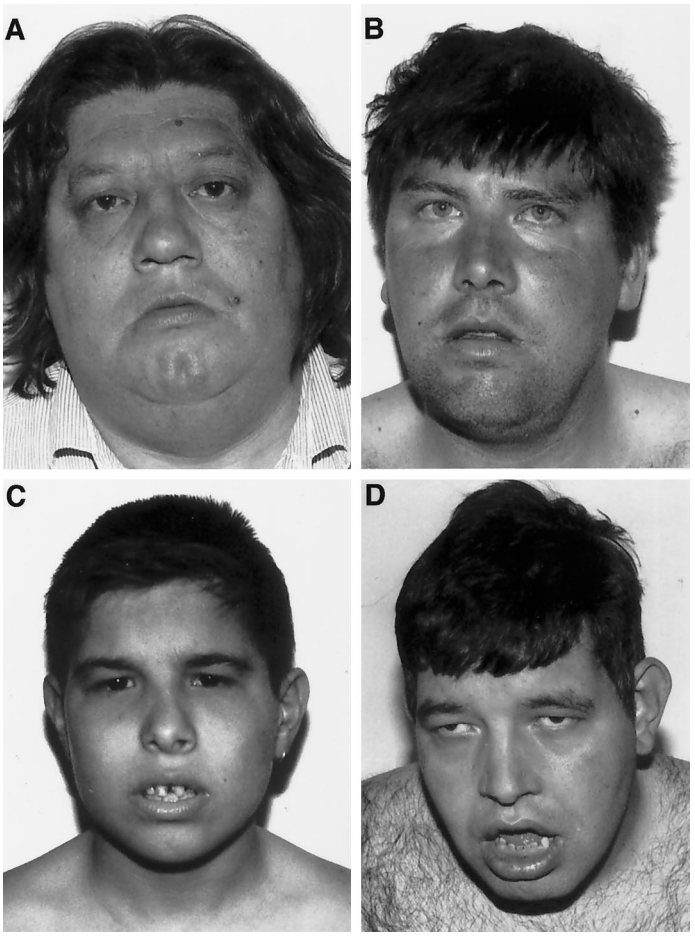

Fig 2. Facial features of the affected male family members. (A) Patient II-16, aged 45 years, exhibiting minor dysmorphic features, including a "carped-shaped" mouth and bulbous nose. (B) Patient II-18, aged 32 years, does not show a distinct facial dysmorphism. (C) Patient III-1, aged 17 years, shows microcephaly, with a small triangular nose, anteverted nares, midface hypoplasia, full lips, and widely spaced incisors. (D) Patient III-10, aged 29 years, has a coarser physiognomy, with midface hypoplasia, the mouth kept open, full lips, and generalized hirsutism.

cluding profound mental retardation, typical facial appearance, urogenital abnormalities, and HbH inclusions.[6] It is becoming increasingly clear that ATR-X syndrome is clinically heterogeneous, however.

Although some features of ATR-X syndrome such as sex reversal appear to breed true within families,[13] others vary both within and between families, even in those family members with identical mutations. For example, we have identified 18 patients from 59 unrelated families with a common (R246C) mutation with considerable variation in phenotype and hematology; the number of cells containing HbH inclusions, a feature of α thalassemia that reflects the degree of imbalance of α and β globin, ranges from 0 to 11% (Gibbons, unpublished data).[11] There may be similar variability within a family.[14,15] Previously, all patients diagnosed with ATR-X syndrome had profound mental retardation; the family presented here provides the first evidence that some patients may have mild mental retardation and, remarkably, live an independent life. Ascertainment bias may explain the previously described rigid association of ATR-X syndrome and profound mental retardation. In the past, only children fitting the original description of the syndrome were referred for analysis. In this pedigree, the 2 older and less severely affected patients had normal developmental milestones and were first brought to medical attention after the onset of epileptic seizures. The ATR-X syndrome was only suspected in adulthood and after it had been clinically diagnosed in 2 younger cousins.

Although the 2 more severely affected boys had the characteristic facial features of ATR-X syndrome, there was no correlation between the degree of mental retardation and the severity of any other clinical or hematological features**.** Similarly, in the past, we have seen no correlation between other clinical features and the degree of α thalassaemia.[16]

ATRX encodes a member of the SNF2 family of adenosine triphosphatase/helicases.[16] Proteins in this group regulate diverse cellular functions, including gene expression, DNA repair, and recombination. They are thought to form multiprotein complexes which influence chromatin and thereby alter the interactions between transacting factors and their cognate binding sites in DNA.[17] It appears that the ATRX protein influences gene expression and that α globin is one of its many normal targets. Presumably, there are several other targets so that mutations of *ATRX* not only cause α

thalassemia but also affect other developmental pathways, including, for example, the nervous and urogenital systems.

It is well known that mutations in similar proteins in yeast and drosophila are very sensitive to polymorphisms in the large number of genes encoding the components of chromatin with which they interact.[18] Also, they are often required in carefully controlled amounts to form multiprotein complexes and therefore might be particularly sensitive to small changes in gene expression. In short, given the nature of the ATRX protein and the complexities of chromatin, one might expect to see considerable variation in the effect of identical mutations from 1 affected individual to another.

This report raises important issues when counseling families at risk from ATR-X syndrome: the phenotype of 1 affected individual might not predict the outcome in subsequent cases.

Might mutations in the *ATRX* gene be found in patients with X-linked mental retardation or in male patients with nonsyndromal mental retardation who previously have not been considered to fall into this diagnostic category? At present, in over 30% of families with all forms of X-linked mental retardation, the disease locus maps to the pericentric region of the X chromosome wherein the *ATRX* gene lies.[19] The current findings suggest that *ATRX* is a plausible candidate in such families. Now that it has been established that the phenotypic spectrum is much wider than previously thought, the full extent of its role in X-linked mental retardation needs to be explored.

This study was supported in part by Italian National Institute of Health research funding (Ministero della Sanità RF 4/96), the Medical Research Council (D.R.H.), and a grant (053014) from the Wellcome Foundation.

We thank the family for their cooperation in this study, Liz Rose and Milly Graver for typing of the manuscript, and Rossana Tonlorenzi for technical assistance. We also thank Prof Sir David Weatherall for his continued support.

References

1. WHO. The ICD-10 classification of mental and behavioural disorders. Clinical description and diagnostic guidelines. Geneva: WHO, 1992
2. Kerr B, Turner G, Mulley J, et al. Non-specific X linked mental retardation. J Med Genet 1991;28:378–382
3. Center for Medical Genetics, Johns Hopkins University, Baltimore, MD, and National Center for Biotechnology Information, National Library of Medicine, Bethesda, MD. Online mendelian inheritance in man (OMIM [TM]). 1999. Available on-line at: http://www.ncbi.nlm.nih.gov/omim/
4. Rousseau F, Heitz D, Tarleton J, et al. A multicenter study on genotype-phenotype correlations in the fragile X syndrome, using direct diagnosis with probe StB12.3: the first 2,253 cases. Am J Hum Genet 1994;55:225–237
5. Gibbons RJ, Picketts DJ, Villard L, Higgs DR. Mutations in a putative global transcriptional regulator cause X-linked mental retardation with α-thalassemia (ATR-X syndrome). Cell 1995; 80:837–845
6. Gibbons RJ, Brueton L, Buckle VJ, et al. The clinical and hematological features of the X-linked α thalassemia/mental retardation syndrome (ATR-X). Am J Med Genet 1995;55:288–299
7. Villard L, Gecz J, Mattéi JF, et al. XNP mutation in a large family with Juberg-Marsidi syndrome. Nat Genet 1996;12: 359–360
8. Wechsler D. Manual for the Wechsler Intelligence Scale for Children–revised. New York: Psychological Corporation, 1974
9. Wechsler D. Wechsler Adult Intelligence Scale–revised. New York: Psychological Corporation, 1981
10. Sparrow SS, Balla DA, Cicchetti DV. Vineland Adaptive Behaviour Scales. Circle Pines, MN: American Guidance Service, 1984
11. Gibbons RJ, Bachoo S, Picketts DJ, et al. Mutations in a transcriptional regulator (hATRX) establish the functional significance of a PHD-like domain. Nat Genet 1997;17:146–148
12. Morisaki H, Morisaki T, Newby LK, Holmes EW. Alternative splicing: a mechanism for phenotypic rescue of a common inherited defect. J Clin Invest 1993;91:2275–2280
13. McPherson E, Clemens M, Gibbons RJ, Higgs DR. X-linked alpha thalassemia/mental retardation (ATR-X) syndrome. A new kindred with severe genital anomalies and mild hematologic expression. Am J Med Genet 1995;55:302–306
14. Lefort G, Taib J, Toutain A, et al. X-linked α-thalassemia/ mental retardation (ATR-X) syndrome. Report of three male patients in a large French family. Ann Genet 1993;36:200–205
15. Logie LJ, Gibbons RJ, Higgs DR, et al. Alpha-thalassaemia mental retardation (ATR-X): an atypical family. Arch Dis Child 1994;70:439–440
16. Picketts DJ, Higgs DR, Bachoo S, et al. *ATRX* encodes a novel member of the SNF2 family of proteins: mutations point to a common mechanism underlying the ATR-X syndrome. Hum Mol Genet 1996;5:1899–1907
17. Kingston RE, Bunker CA, Imbalzano AN. Repression and activation by multiprotein complexes that alter chromatin structure. Genes Dev 1996;10:905–920
18. Pirrotta V. PcG complexes and chromatin silencing. Curr Opin Genet Dev 1997;7:249–258
19. Schwartz CE. X-linked mental retardation: in pursuit of a gene map. Am J Hum Genet 1993;52:1025–1031 (Editorial)

Endothelin-1 in the Brain of Patients with Galactosialidosis: Its Abnormal Increase and Distribution Pattern

Kohji Itoh, PhD,* Kiyomitsu Oyanagi, MD, PhD,† Hitoshi Takahashi, MD, PhD,‡ Takeshi Sato, MD, PhD,§ Yoshio Hashizume, MD, PhD,‖ Michie Shimmoto, MS,* and Hitoshi Sakuraba, MD*

Endothelin-1 is a peptidic substrate in vitro of lysosomal protective protein/cathepsin A (PPCA) with serine carboxypeptidase activity. Endothelin-1–specific immunoreactivity has been demonstrated to be markedly increased and distributed abnormally in the neurons and glial cells within autopsied brain regions, including the cerebellum, hippocampal formation, and spinal cord, of patients affected with galactosialidosis, a human PPCA deficiency. The genetic defect of the endothelin-1 degrading activity of PPCA is suggested to cause some of the neurological abnormalities of this disease.

Itoh K, Oyanagi K, Takahashi H, Sato T, Hashizume Y, Shimmoto M, Sakuraba H. Endothelin-1 in the brain of patients with galactosialidosis: its abnormal increase and distribution pattern. Ann Neurol 2000;47:122–126

Lysosomal protective protein/cathepsin A (PPCA) is a multifunctional glycoprotein that regulates the expression of neuraminidase and β-galactosidase through the formation of a multienzymatic complex in lysosomes[1,2] and also exhibits serine esterase activities (acid carboxypeptidase [cathepsin A] and neutral esterase/deamidase) against the carboxyl termini of a subset of neuropeptides, including endothelin-1 (ET-1).[3–6]

ET-1, initially characterized as a potent vasoconstrictive peptide,[7] exerts diverse functions in both vascular and nonvascular tissues,[8] through binding to ET receptors A and B with different affinities.[9] The carboxyl terminal amino acid residues of ET-1 are essential for expression of its biological activities.[10]

Galactosialidosis (GS) is a human PPCA deficiency characterized by a simultaneous decrease in lysosomal neuraminidase and β-galactosidase activities associated with consequent storage of sialylated oligosaccharides and glycolipids in tissues and urine[1,11–14] as well as serine esterase activities.[15,16] Most patients develop loss of vision as an initial symptom at the age of 10 to 15 years, followed by neurosomatic abnormalities, including cerebellar ataxia, action myoclonus, cherry-red spots, coarse facies, angiokeratoma, and visceromegaly (juvenile/adult form).[11–14] So far, however, the pathophysiological role of the catalytic function of PPCA remains to be elucidated.

We report here the abnormal distribution of ET-1 as a potential natural substrate in the brain tissue from patients with a deficiency of PPCA manifesting as a serine carboxypeptidase.

Patients and Methods

Patients

The clinical and biochemical data on the 3 patients with the juvenile/adult form of GS have been reported.[12–14,17] Briefly, Patient 1,[13] a Japanese boy with consanguineous parents, was noted to have mental retardation as an initial symptom at 5 years of age and then developed a coarse face, visual disturbance, hyperreflexia, and cerebellar ataxia at the age of 9 years. By the age of 12 years, severe muscle atrophy, action myoclonus, and convulsive seizures had progressed. At the age of 13 years, a tracheostomy was performed, but the patient died of tracheal bleeding.

Patient 2,[17] a Japanese man with consanguineous parents, was diagnosed at the age of 20 years with visual disturbance and slight mental retardation as the initial symptoms. He was noted to have a cerebellar ataxia at the age of 31 years and then developed visual disturbance, hyperreflexia, ataxic gait, muscle atrophy, and myoclonic and convulsive seizures by the age of 40 years. His manifestations further progressed, and the patient died at the age of 42 years.

Patient 3,[12] a Japanese man with nonconsanguineous parents, developed moderate visual disturbance at the age of 22 years and was diagnosed at the age of 32 years with low normal intelligence and changes in emotional and behavioral activities, angiokeratoma, and mild dysmorphic manifestations. His neurological abnormalities slowly developed. He died at the age of 43 years as the result of injuries sustained in a traffic accident.

A male patient with Krabbe disease with lysosomal disease other than GS diagnosed by typical clinical manifestations and a deficiency of galactocerebrosidase, who died at the age of 2 years, was included as a pathological control.

Immunohistochemistry

Consecutive sections (6-μm thickness) embedded in paraffin were prepared from the autopsied brain tissues from control

From the *Department of Clinical Genetics, The Tokyo Metropolitan Institute of Medical Science, Tokyo Metropolitan Organization for Medical Research and †Department of Neuropathology, Tokyo Metropolitan Institute for Neuroscience, Tokyo, ‡Department of Pathology, Brain Research Institute, Niigata University, Niigata, §Kohnodai Hospital, National Center of Neurology and Psychiatry, Chiba, and ‖Institute for Medical Science of Aging, Aichi Medical University, Aichi, Japan.

Received Jun 21, 1999, and in revised form Aug 16, 1999. Accepted for publication Aug 19, 1999.

Address correspondence to Dr Itoh, Institute for Medicinal Resources, Faculty of Pharmaceutical Sciences, University of Tokushima, 1-78 Shomachi, Tokushima 770-8505, Japan.

subjects (aged 15, 39, and 42 years), the patient with Krabbe disease (aged 2 years), and 3 patients with the juvenile/adult form of GS (aged 13, 42, and 43 years).[12–14,17] After deparaffinization and rehydration, the sections were treated with 0.3% H_2O_2 in methanol for 30 minutes and then heated in Target Unmasking Fluid reagent (PharMingen, San Diego, CA) at 90°C for 5 minutes in a microwave oven for restoration of the antigenicity. After blocking with 10% normal goat serum in 0.01 M of phosphate-buffered (0.15-M) saline (PBS) (pH 7.4), diluted affinity purified polyclonal antibodies, anti-PPCA (10 μg/ml), anti–ET-1 (5 μg/ml), and anti–ET-3 (5 μg/ml) were alternately applied to the sections overnight at 4°C. In another experiment, anti–ET-1 (1 μg/ml) premixed with authentic ET-1 (4 μg/ml; Sigma, St Louis, MO) was applied to the adjacent sections. Anti-PPCA is a rabbit polyclonal IgG against the N-terminal oligopeptide of the 32-kd subunit of human PPCA previously prepared.[18] Rabbit anti–ET-1 and anti–ET-3 polyclonal IgGs were purchased from Immuno-Biological Laboratories (Gunma, Japan). The sections were washed with PBS containing 0.05% Tween 20 (Bio-Rad, Hercules, UK) and incubated with a biotinylated antibody to rabbit IgG (Vector, Burlingame, CA) (1:1,000 dilution) for 1 hour at room temperature and then with streptoavidin-conjugated horseradish peroxidase (Histofine SAB-PO kit; Nichirei Company, Tokyo, Japan) for 30 minutes at room temperature. After washing with PBS containing 0.5% Tween 20, the horseradish peroxidase reaction was performed with 0.05% 3,3′–diaminobenzidine tetrahydrochloride (GIBCO-BRL, Grand Island, NY) and 0.0015% H_2O_2 for 3 minutes. The specimens were then counterstained with Mayer's hematoxylin solution and viewed under an Axiophot light microscope (Zeiss, Oberkochen, Germany).

Results

Immunohistochemical Analysis of PPCA and ET-1

In the cerebella of control subjects, PPCA was found as dense granular immunoreactive structures distributed in the cell bodies and dendrites of neurons of the cortex and dentate nucleus, including Purkinje, Golgi, basket, outer stellate, and granule cells (Fig 1A and G).

Fig 1. Immunohistochemical localization of lysosomal protective protein/cathepsin A (PPCA), endothelin-1 (ET-1), and ET-3 in the human cerebellar cortex and dentate nucleus. The PPCA immunoreactivity (brown) in a 15-year-old control subject was mainly distributed in Purkinje and Golgi cells as well as in basket and outer stellate cells of the molecular layer. Fine granular immunostaining was observed in granule cells. (A) Less PPCA immunoreactivity was detected in glial cells. (B) No PPCA immunoreactivity was observed in the cortex of 13-year-old galactosialidosis (GS) Patient 1 (PPCA deficiency), indicating the specificity of the anti-PPCA antibody. With the exception of a few Golgi cells (arrowhead)*, ET-1 immunoreactivity was barely observed in control sections from the 15-year-old male patient (C) and a 2-year-old male patient with Krabbe disease (galactocerebrosidase deficiency) (E). ET-1 immunoreactivity (brown color) was found to be abnormally distributed in ballooned Golgi cells as well as in basket and outer stellate cells of the molecular layer of 13-year-old GS Patient 1 (D) and 42-year-old GS Patient 2 (F). Bergmann glial cells were also ET-1–positive. The molecular layer was diffusely immunopositive as shown in panel D. Granular PPCA immunoreactivity (brown) was mainly distributed in the somatic regions of the dentate nuclear neurons in a 15-year-old control subject. (G) Weak PPCA immunoreactivity was detected in glial cells. (H) No PPCA immunoreactivity was observed in the neurons of 13-year-old GS Patient 1. (I) A weak ET-1 immunoreactivity (brown) was observed in the neurons of a 15-year-old control subject. (J) ET-1 immunoreactivity was found to be markedly increased in the somatic regions of dentate nuclear neurons of 13-year-old GS Patient 1. ET-3 immunoreactivity was not observed in either the control subject (K) or Patient 1 (L). (M) Low-magnification view of the dentate nucleus of Patient 1 labeled with 1 μg/ml of affinity-purified anti–ET-1 antibody. (N) Adjacent section of dentate nucleus of Patient 1 stained with 1 μg/ml of anti–ET-1 antibody in the presence of 4 μmg/ml of authentic ET-1 peptide. The 6-μm-thick sections were processed as described in the Patients and Methods section. The scale bars in the panels correspond to 50 μm. (Original magnification, ×720 in A–D and G–J; ×1,000 in E, F, K, and L; and ×400 in M and N.)*

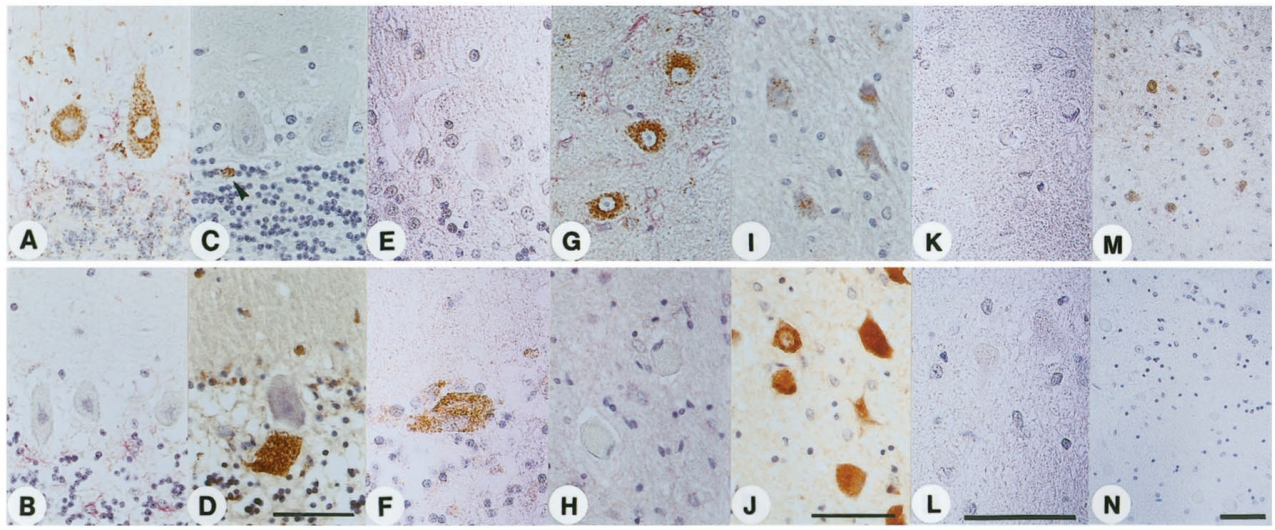

A small number of Bergmann glia as well as astrocytic and oligodendroglial cells showed fine granular weak but evident immunostaining (see Fig 1A and G). In contrast, the cerebellum of GS patients showed completely negative PPCA immunoreactivity (IR) in the same regions (see Fig 1B and H), where the two characteristics of neuronal loss with fibrillary gliosis in the Purkinje or granule cell layer and marked ballooning of Golgi cells and neurons of the dentate nucleus were seen.[13]

On the other hand, significant ET-1 IR was found in the Golgi, basket, and outer stellate cells; Bergmann glia of the cortex (see Fig 1D and F); and neurons of the dentate nucleus (see Fig 1J and M), having a rather swollen shape. Weak but evident ET-1 IR was detected in some parts of astrocytes in the white matter and granule cells. The distribution of ET-1 IR in GS was similar to that of PPCA in the control subjects, although the reactivity was less in the Purkinje cells of the patients. Age-dependent changes were not observed, however. In contrast, a relatively small amount of ET-1 was present in a few Golgi cells and the neurons of the dentate nucleus of the control subjects (see Fig 1C and I), indicating that these cells physiologically produce ET-1. ET-3 IR could not be observed in the cerebella (see Fig 1K and L). Furthermore, competitive inhibition of the ET-1 immunostaining of the sections from GS patients with an excess amount of the authentic ET-1 revealed the specificity of the ET-1 IR (see Fig 1N).

Such an abnormal distribution of ET-1 was also observed in other brain regions, including the spinal cord (Fig 2) and hippocampal formation (Fig 3). In the spinal cord of control subjects, PPCA was highly expressed in the anterior horn cells (see Fig 2A), although weak ET-1–specific IR was observed in the same cell population of controls (see Fig 2C). In contrast, some but not all of the anterior horn cells showed a marked increase of ET-1 IR in the somatic regions of a GS patient (see Fig 2D), although the neurons did not show the presence of PPCA (see Fig 2B). In the hippocampal formation of control subjects, a relatively small amount of ET-1 IR was observed in pyramidal neurons of the CA-1 region and dentate gyrus (see Fig 3A and C). On the other hand, a significant increase of ET-1 IR in GS was observed in the same cell populations affected with GS (see Fig 3B and D), which was also observed in the CA-2 and CA-3 regions (data not shown). The findings obtained from a Krabbe disease case included as a pathological control were identical to those of the normal subjects.

Discussion

This is the first demonstration that ET-1 IR is distributed abnormally and apparently accumulates in the subpopulations of neurons and glial cells affected with GS (a PPCA deficiency). Previous neuropathological analyses of the GS patients revealed heterogeneous storage materials, including glycoconjugates with sialyloligosaccharides and phospholipids, in their brains.[13] In this study, ET-1 as a possible natural substrate of PPCA has been newly identified as one of the storage materials in the cerebellum, hippocampus, and spinal cord. Furthermore, the immunohistochemical changes were specific for ET-1 but not for ET-3.

ET-1 is widely expressed and distributed in neurons and glia as well as in vascular cells within various brain regions,[8,9] including the cerebral cortex, striatum, hippocampus, pituitary gland, hypothalamus, cerebellum, and spinal cord. The most active mature form (ET-1: 21 amino acids) is produced from a prepro type precursor (prepro–ET-1: 212 amino acids) via an intermediate form (big ET-1: 38 amino acids) through highly specific proteolytic processing by a furin-like convertase and endothelin-converting enzymes.[7,8] In vascular endothelial cells, ET-1, once synthesized, is secreted via the constitutive exocytotic pathway.[10] In contrast, ET-1 is stored as a mature form in motoneurons of the spinal cord and paraventricular nuclear neurons of the posterior pituitary gland.[19] It is released from nerves by external stimuli, acts on both neurons and glia through binding to ET receptors, and modulates the signal

Fig 2. Immunodetection of lysosomal protective protein/cathepsin A (PPCA) and endothelin-1 (ET-1) in the anterior horn of the spinal cord. (A) Granular PPCA immunoreactivity (brown) was distributed mainly in the somatic regions of the anterior horn cells in a 42-year-old control subject. (B) No PPCA immunoreactivity was observed in the neurons of 43-year-old galactosialidosis (GS) Patient 3. (C) Weak ET-1 immunoreactivity (brown) was observed in the anterior horn cells of the control subject. (D) Neurons with a marked increase of ET-1 immunoreactivity in the somatic regions were observed in Patient 3. The 6-mm-thick sections were processed as described in the Patients and Methods section. Scale bar = 50 μm.

Fig 3. Differential levels of endothelin-1 (ET-1) immunoreactivity in the hippocampus of a 42-year-old control (A and C) and 43-year-old galactosialidosis (GS) Patient 3 (B and D). All sections were labeled with 5 μg/ml of anti–ET-1 antibody. CA-1 regions of the hippocampus are shown in A and CA-4 regions and the dentate gyrus are shown in C and D. The patient's pyramidal neurons in the CA-1 and CA-4 regions exhibit intense granular ET-1 immunoreactivity (brown) in their cytoplasm. A weak but significant increase in ET-1 immunoreactivity was observed in the neurons of the dentate gyrus affected with GS in D. Scale bar = 100 μm.

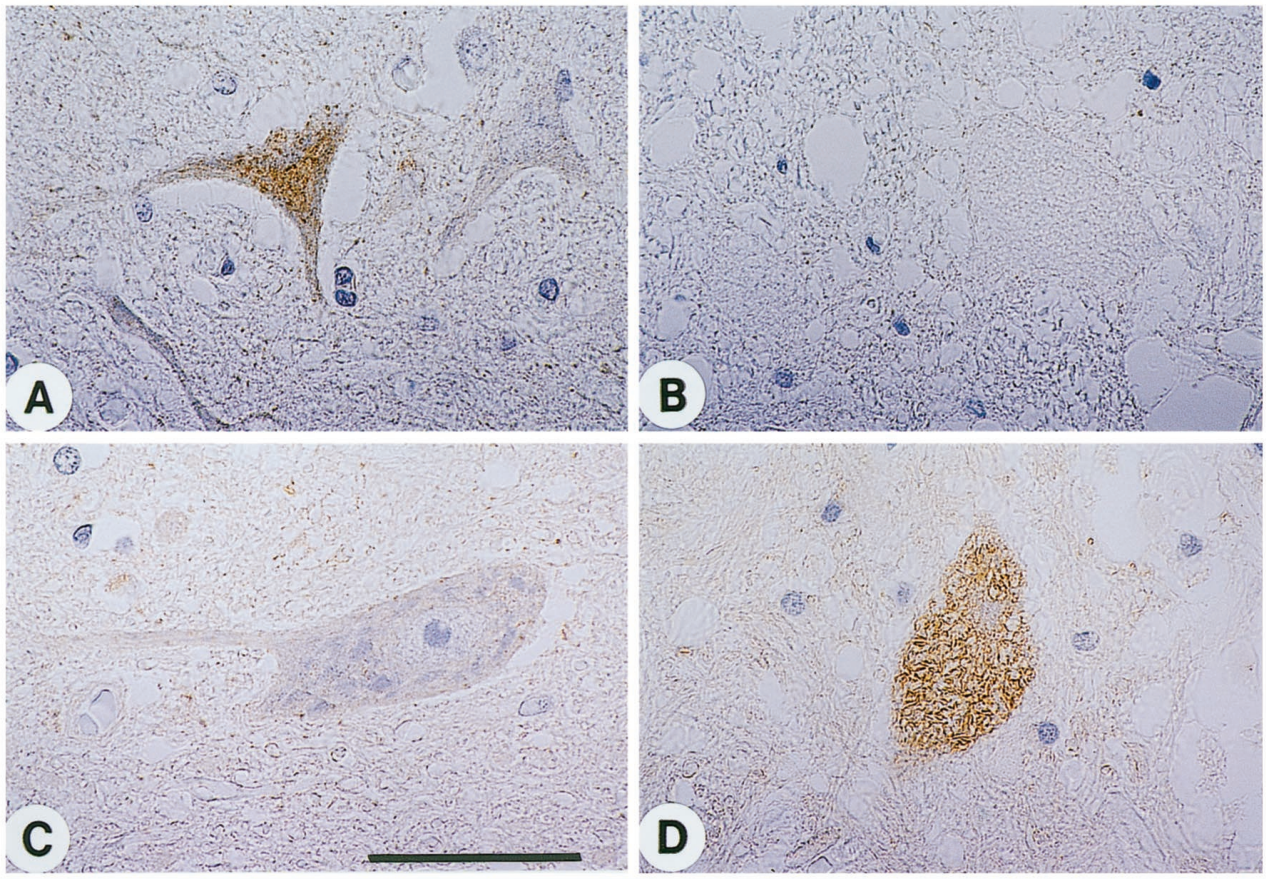

Fig 2

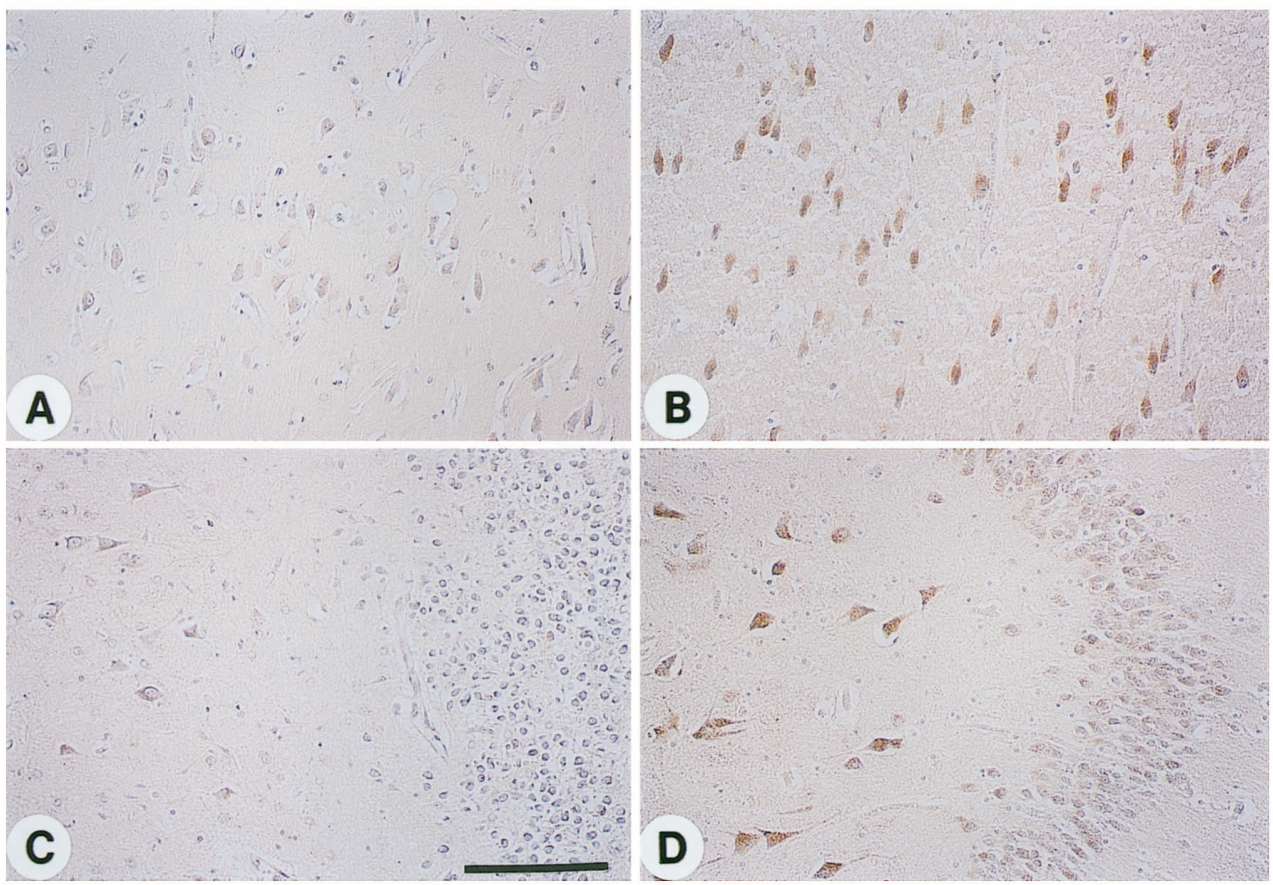

Fig 3

transduction system to cause neuronal excitation and glial cell mitogenesis.[9,19,20] As PPCA inactivates ET-1 by degrading its carboxyl terminus,[6,16] the catalytic defect of PPCA may thereby increase the local concentration of ET-1 available for receptor binding and signal transduction. The integral stimulation of ET receptors on neurons or glia may disrupt normal cellular homeostasis, potentially leading to the degeneration of neurons or to the abnormal proliferation of glia.

In recent years, PPCA has been shown to modify in vitro the carboxyl termini of a variety of physiologically active peptides with hydrophobic amino acid residues, including substance P, neurokinins, bradykinin, oxytocin, and vasopressin.[5] Therefore, determination of the biological and clinical significance of the loss of the catalytic function of PPCA in GS may present us with a novel model for studies aimed at elucidating the relation between the abnormal catabolism of both ET-1 and other neuropeptides in the nervous system and the pathogenesis of the neurological manifestations in GS.

This work was supported by grants from the Ministry of Education, Science, and Culture of Japan; the Ministry of Welfare and Health of Japan; and the Suzuken Memorial Foundation.

The authors thank Prof T. Miyatake (Showa College of Pharmaceutical Sciences, Tokyo, Japan) for the valuable advice.

References

1. d'Azzo A, Hoogeveen AT, Reuser AJJ, et al. Molecular defect in combined β-galactosidase and neuraminidase deficiency in man. Proc Natl Acad Sci USA 1982;79:4535–4539
2. Galjart NJ, Gillemans N, Harris A, et al. Expression of cDNA encoding the human "protective protein" associated with lysosomal β-galactosidase and neuraminidase: homology to yeast proteases. Cell 1988;54:755–764
3. Tranchemontagne J, Michaud L, Potier M. Deficient lysosomal carboxypeptidase activity in galactosialidosis. Biochem Biophys Res Commun 1990;168:22–29
4. Itoh K, Takiyama N, Kase R, et al. Purification and characterization of human lysosomal protective protein expressed in stably transformed Chinese hamster ovary cells. J Biol Chem 1993;268:1180–1186
5. Jackman HL, Tan F, Tamei H, et al. A peptidase in human platelets that deamidates tachykinins. Probable identity with the lysosomal "protective protein." J Biol Chem 1990;256:11256–11272
6. Jackman HL, Morris PW, Rabito SF, et al. Inactivation of endothelin-1 by an enzyme of the vascular endothelial cells. Hypertension 1993;21:925–928
7. Yanagisawa M, Kurihara H, Kimura S, et al. A novel potent vasoconstrictor peptide produced by vascular endothelial cells. Nature 1988;332:411–415
8. Masaki T, Yanagisawa M. Molecular biology and biochemistry of the endothelins. Trends Pharmacol Sci 1989;10:374–378
9. Kuwaki T, Kurihara H, Cao WH, et al. Physiological role of brain endothelin in the central autonomic control: from neuron to knockout mouse. Prog Neurobiol 1997;51:545–579
10. Kimura S, Kasuya Y, Sawamura T, et al. Structure-activity relationships of endothelin: importance of the C-terminal moiety. Biochem Biophys Res Commun 1988;156:1182–1186
11. d'Azzo A, Andria G, Striscriuglio P, Galjaard H. Galactosialidosis. In: Scriver CR, Beaudet AL, Sly WS, Valle D, eds. The metabolic and molecular bases of inherited disease. 7th ed. New York: McGraw-Hill, 1995:2825–2837
12. Suzuki Y, Sakuraba H, Yamanaka T, et al. Galactosialidosis: a comparative study of clinical and biochemical data on 22 patients. In: Arima M, Suzuki Y, Yabuuchi H, eds. The developing brain and its disorders. Tokyo: University of Tokyo Press, 1984:161–175
13. Oyanagi K, Ohama E, Miyashita K, et al. Galactosialidosis: neuropathological findings in a case of the late-infantile type. Acta Neuropathol (Berl) 1991;82:331–339
14. Shimmoto M, Fukuhara Y, Itoh K, et al. Protective protein gene mutations in galactosialidosis. J Clin Invest 1993;91:2393–2398
15. Kase R, Itoh K, Takiyama N, et al. Galactosialidosis: simultaneous deficiency of esterase, carboxyl-terminal deamidase and acid carboxypeptidase activities. Biochem Biophys Res Commun 1990;172:1175–1179
16. Itoh K, Kase R, Shimmoto M, et al. Protective protein as an endogenous endothelin degradation enzyme in human tissues. J Biol Chem 1995;270:515–518
17. Koga M, Sato T, Ikuta F, et al. An autopsy case of familial neurovisceral storage disease of late onset. Folia Psychiatr Neurol Jpn 1978;32:299–308
18. Satake A, Itoh K, Shimmoto M, et al. Distribution of lysosomal protective protein in human tissues. Biochem Biophys Res Commun 1994;205:38–43
19. Lee M-E, dela Monte SM, Ng S-C, et al. Expression of the potent vasoconstrictor endothelin in the human central nervous system. J Clin Invest 1990;86:141–147
20. Giaid A, Gibson SJ, Ibrahim NBN, et al. Endothelin-1, an endothelium-derived peptide, is expressed in neurons of the human spinal cord and dorsal root ganglia. Proc Natl Acad Sci USA 1989;86:7634–7638

Combination Therapy with Glatiramer Acetate (Copolymer-1) and a Type I Interferon (IFN-α) Does Not Improve Experimental Autoimmune Encephalomyelitis

Staley A. Brod, MD, J. William Lindsey, MD, and Jerry S. Wolinsky, MD

We sought to determine whether combinations of glatiramer acetate and parenteral or ingested type I interferon were synergistic in experimental autoimmune encephalomyelitis. Glatiramer acetate, subcutaneous murine interferon-α, or ingested murine interferon-α individually improved clinical scores. In contrast, glatiramer acetate in conjunction with either subcutaneous or ingested interferon-α did not improve clinical scores compared with control. These data suggest that clinical trials designed to test a possible synergistic effect of glatiramer acetate and type I interferon in humans should be designed to detect possible adverse effects of this combination of immunomodulatory agents.

Brod SA, Lindsey W, Wolinsky JS. Combination therapy with glatiramer acetate (copolymer-1) and a type 1 interferon (IFN-α) does not improve experimental autoimmune encephalomyelitis. Ann Neurol 2000;47:127–131

Parenteral type I interferon (IFN-α2 [Roferon], IFNβ-1a [Avonex/Rebif], and IFNβ-1b [Betaseron]) and glatiramer acetate (copolymer-1 [Copaxone]) decrease the number of clinical attacks in relapsing-remitting multiple sclerosis (MS) by 17 to 32%.[1–5] IFNα-2a treatment results in fewer new magnetic resonance imaging lesions during the treatment period.[6] Because each therapy alone has a partial therapeutic benefit, a clinical trial to determine if combined use of a parenteral IFNβ-1a (Avonex) and glatiramer acetate is additive or synergistic is underway.[7] Experimental autoimmune encephalomyelitis (EAE) is a T-cell mediated inflammatory autoimmune process of the central nervous system (CNS) which resembles the human demyelinating disease MS in some aspects and provides a model to assess the therapeutic interventions that may influence its course.[8] We have demonstrated that ingested IFN-α can modify biological responses in chronic relapsing EAE in SJL/J mice and acute EAE in Lewis rats.[9] Ingested type 1 interferon is more effective than parenteral (subcutaneous) IFN-α in the suppression of attacks in chronic relapsing EAE.[10] The EAE model may provide insight into the clinical potential of glatiramer acetate and type I interferon combinations and aid in the design of clinical trials. Therefore, we determined whether combinations of glatiramer acetate and parenteral or ingested type I interferon are synergistic in EAE.

From the Department of Neurology and Multiple Sclerosis Research Group, University of Texas Health Science Center at Houston, Houston, TX.

Received Jul 9, 1999, and in revised form Aug 23. Accepted for publication Aug 27, 1999.

Address correspondence to Dr Brod, Department of Neurology, Multiple Sclerosis Research Group, MSMB 7.044, University of Texas at Houston, Health Science Center, PO Box 20708, Houston, TX 77225.

Experimental Methods

In the initial experiments to establish the efficacy of optimal dosing of glatiramer acetate for use in combined intervention experiments, SJL/J mice (n = 8–12 per group) received either 10, 5, or 1 mg of glatiramer acetate (Teva Pharmaceutical Industries, Israel) in incomplete Freund's adjuvant (IFA), and a control group received a mock injection of saline in IFA 3 weeks preceding inoculation (day 0). On day 0, all mice were inoculated with 0.2 mg of encephalitogen (lyophilized mouse spinal cord homogenate [MSCH]) in complete Freund's adjuvant (CFA) and scored by a blinded observer for 21 to 28 days after inoculation. This is the typical prevention experimental model to evaluate glatiramer acetate batch efficacy.[11]

In the second set of three separate experiments, CSJL/F1 or SJL/J mice were divided into two different groups of 24 mice each. The first group received a suboptimal but therapeutic single dose of 1 mg of glatiramer acetate in IFA, and the other group received a mock injection of saline in IFA 3 weeks preceding inoculation (day 0). A suboptimal glatiramer acetate dose was used to enable the detection of any potential additive or synergistic effect of parenteral or ingested type 1 interferon without resorting to excessive numbers of experimental mice to demonstrate such an effect. Beginning at day −7 through and including day +14, 8 mice in each group received either 100 IU of murine IFN-α subcutaneously (Cytimmune mouse IFN-α, 4×10^5 IRU/ml; Lee Biomolecular Research, San Diego, CA) or 10 IU of murine IFN-α by gavage. IFN-α doses were chosen to provide optimal protection in this model. On day 0, all mice were inoculated with 0.2 mg of encephalitogen MSCH, proteolipid protein (PLP) 139–151 peptide, or PLP 178–191 peptide in CFA and were scored by a blinded observer for at least 17 days after inoculation. Spleen cells were cultured with Con A (2.5 mg/ml), *Mycobacterium tuberculosis*, PLP 139–151 at 2 to 20 μg/ml, glatiramer acetate at 3 to 30 μg/ml at 2×10^5 cells per well in 96 round-bottom well

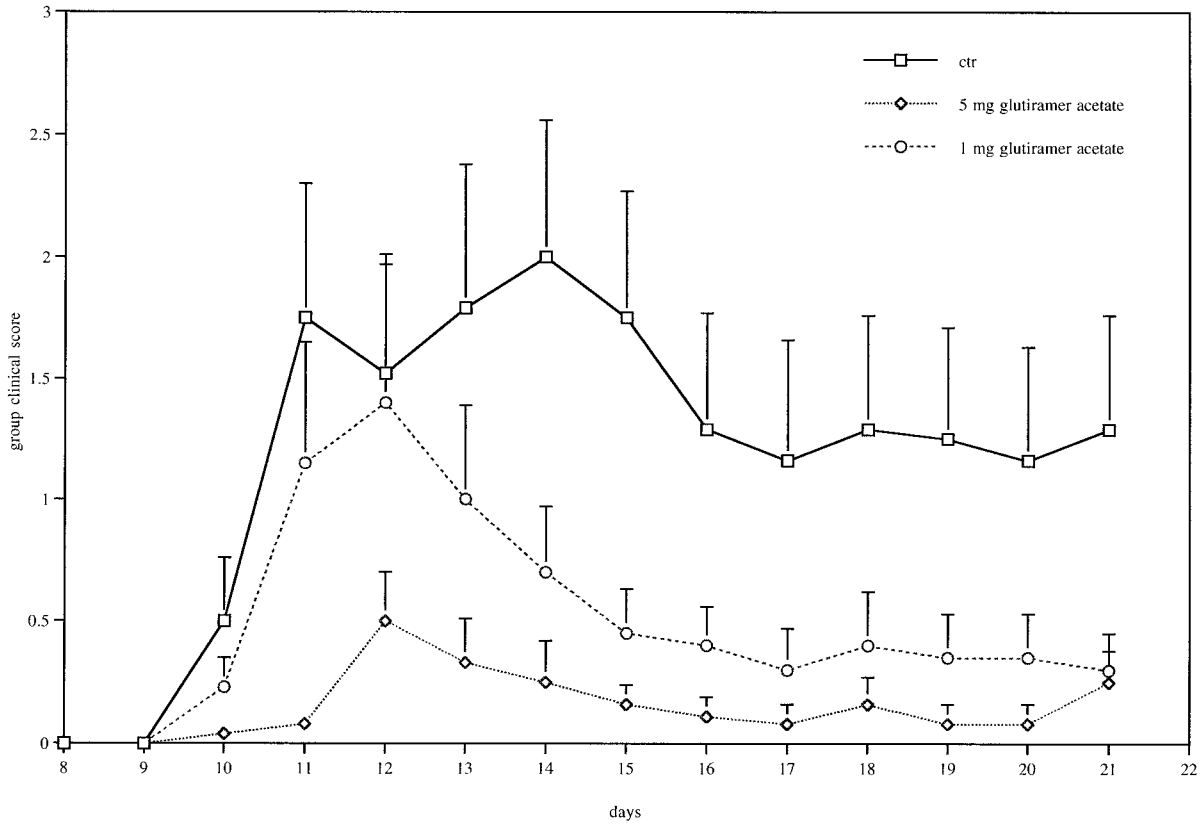

Fig 1. One milligram of glatiramer acetate acts suboptimally in protection against experimental autoimmune encephalomyelitis. SJL/J mice (n = 8 per group) received either 5 or 1 mg of glatiramer acetate in incomplete Freund's adjuvant (IFA), and the control group received a mock injection of saline in IFA 3 weeks preceding inoculation (day 0) with lyophilized mouse spinal cord homogenate (MSCH) in complete Freund's adjuvant (CFA). On day 0, all mice were inoculated with 0.2 mg of MSCH in CFA and were scored by a blinded observer for 21 days after inoculation. Clinical severity of the initial attack was graded as follows by a blinded observer: 0 = no disease, 1 = limp tail or slow righting response, 2 = limp tail and slow righting response, 3 = paraparesis with abnormal gait, 4 = paraplegia but mobile using forelimbs, 5 = inanition, 6 = dead. Mice were scored daily, and a cumulative score was computed by averaging scores for each group of animals ± SEM.

plates in a humidified 5% carbon dioxide and 95% air incubator at 37°C. Supernatants were collected at 48 hours and frozen at −70°C after centrifugation. Interleukins were measured using solid-phase enzyme-linked immunosorbent assay with anti–interleukin-2 (IL-2), anti–IL-4, anti–IL-6, anti–IL-10, anti–tumor necrosis factor-α, anti–transforming growth factor-β, or anti–IFN-γ (PharMingen, San Diego, CA) antibodies as outlined previously.[9]

Results and Discussion

We first determined if previously described effective doses of glatiramer acetate were effective in suppressing

Fig 2. Combination therapy with glatiramer acetate and interferon-α (IFN-α) does not improve experimental autoimmune encephalomyelitis. (A) In the first set of experiments, CSJL/J F1 or SJL/J mice were divided into two different groups of 24 mice each. The first group received 1 mg of glatiramer acetate in incomplete Freund's adjuvant (IFA), and the other group received a mock injection of saline in IFA 3 weeks preceding inoculation (day 0). Beginning at day −7 through and including day +14, 8 mice in each group received either 100 IU of murine IFN-α subcutaneously or 10 IU of murine IFN-α by gavage. On day 0, all mice were inoculated with 0.2 mg of encephalitogen (lyophilized mouse spinal cord homogenate [MSCH]) in complete Freund's adjuvant (CFA) and were scored by a blinded observer for at least 15 days after inoculation. (B) In cumulative results from three separate experiments, CSJL/J F1 or SJL/J mice were divided into two different groups of 72 mice each. The first group received 1 mg of glatiramer acetate in IFA, and the other group received a mock injection of saline in IFA 3 weeks preceding inoculation (day 0). Beginning at day −7 through and including day +14, 24 mice in each group received either 100 IU of murine IFN-α subcutaneously or 10 IU of murine IFN-α by gavage. On day 0, all mice were inoculated with 0.2 mg of encephalitogen (MSCH, proteolipid protein [PLP] 139–151 peptide, or PLP 178–191 peptide) in CFA and were scored by a blinded observer for at least 17 days after inoculation.

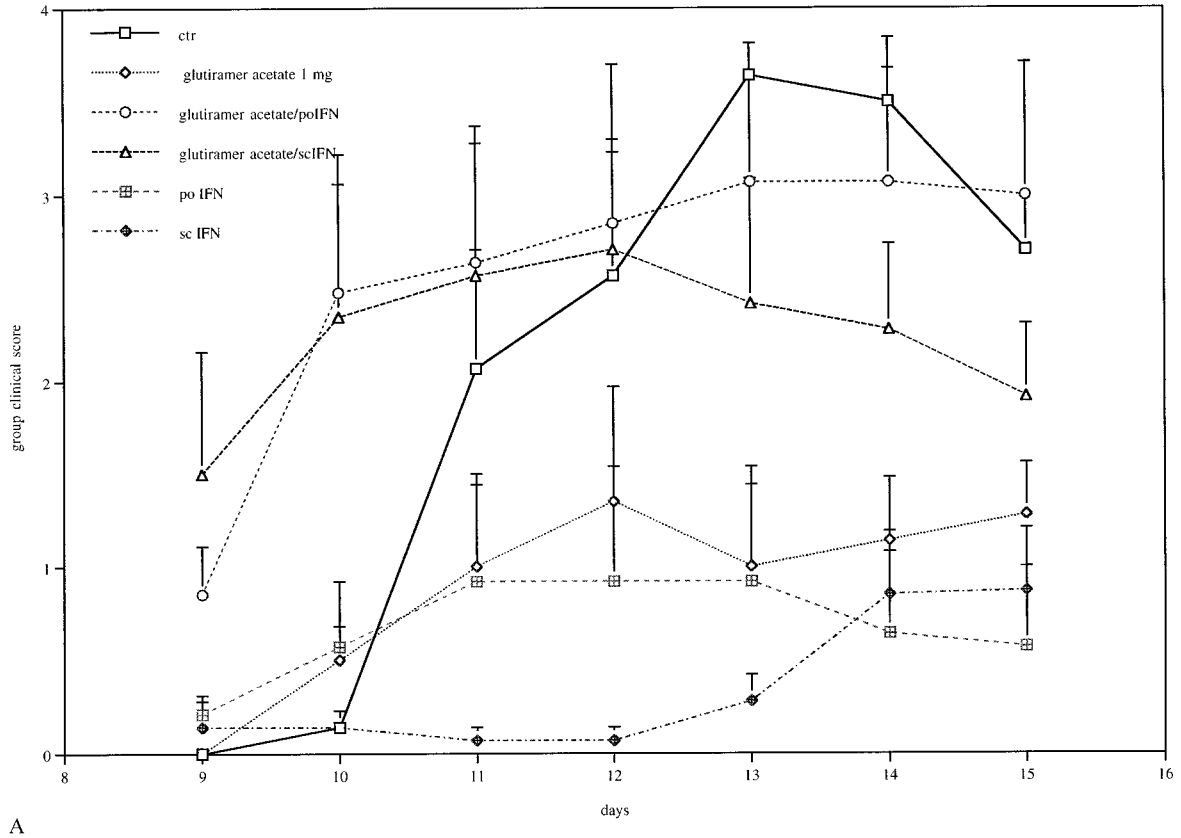
ctr
glutiramer acetate 1 mg
glutiramer acetate/poIFN
glutiramer acetate/scIFN
po IFN
sc IFN
group clinical score
days
0
1
2
3
4
8
9
10
11
12
13
14
15
16

A

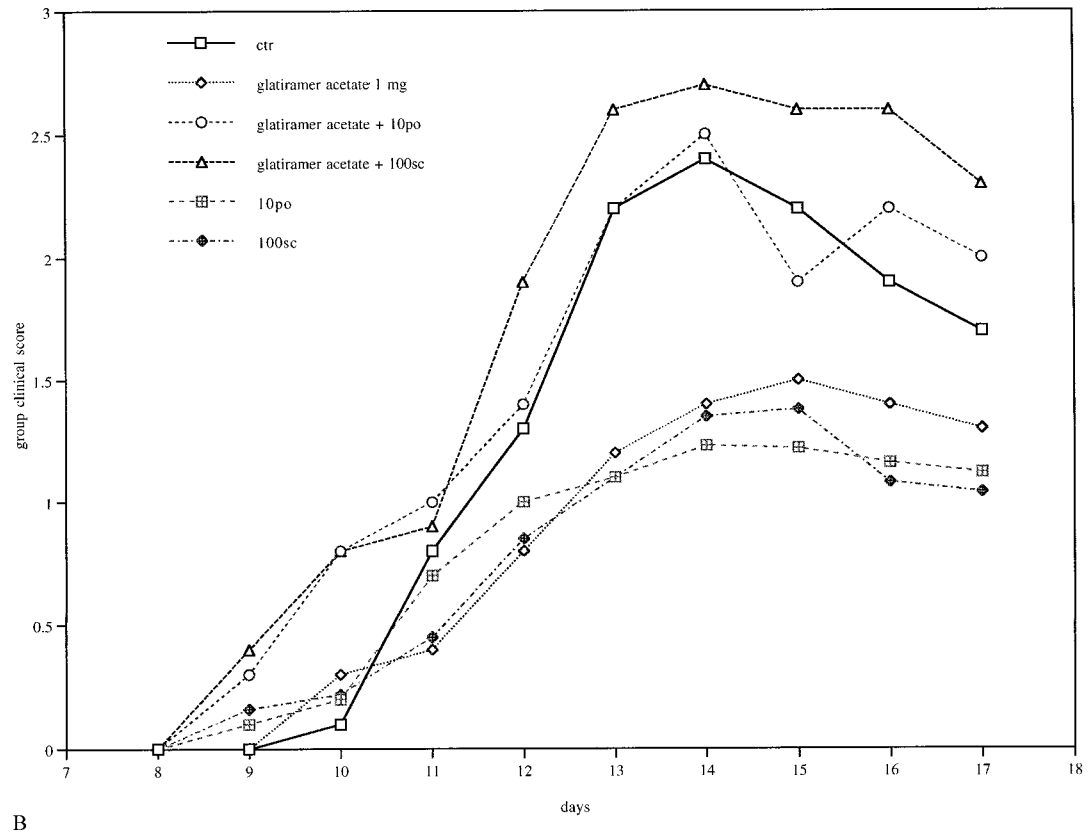
ctr
glatiramer acetate 1 mg
glatiramer acetate + 10po
glatiramer acetate + 100sc
10po
100sc
group clinical score
days
0
0.5
1
1.5
2
2.5
3
7
8
9
10
11
12
13
14
15
16
17
18

B

EAE. We performed an initial set of experiments in which mice received either 10 mg of glatiramer acetate in IFA or a mock injection of saline in IFA 3 weeks preceding inoculation with MSCH (day 0). Mice receiving an optimal dose of glatiramer acetate (group clinical score: 4.3 ± 0.6 [SE]) had much less severe clinical disease compared with the control group (group clinical score: 0.8 ± 0.4 [SE]). Based on these results, sample size projections to determine a 50% or greater additive effect of IFN-α on clinical outcome projected the requirement of 200 mice per study arm. Therefore, to demonstrate any potential additive or synergistic effect and to more readily detect any deleterious effect of parenteral or ingested type 1 interferon used in combination with glatiramer acetate, we sought a suboptimal glatiramer acetate dose. Additional experiments were performed with glatiramer acetate alone in which mice received either 5 or 1 mg of glatiramer acetate in IFA or a mock injection of saline in IFA 3 weeks preceding inoculation with MSCH (day 0). The 5-mg dose still provided good protection against EAE, whereas the 1-mg dose was less effective, particularly early in the course of disease (Fig 1). Therefore, we used the 1-mg glatiramer acetate dose in experiments modeling combined treatment with either parenteral or ingested IFN-α.

Subsequently, we examined the effect of combinations of 1 mg of glatiramer acetate and optimal subcutaneous or ingested IFN-α doses in mice inoculated as described above. In the first set of experiments, control, glatiramer acetate and ingested IFN-α, and glatiramer acetate and subcutaneous IFN-α all showed at least a mean group clinical score of 2.5, whereas the glatiramer acetate, subcutaneous murine IFN-α, and ingested murine IFN-α individually had mean group clinical scores no greater than 1.3 (Fig 2A). In the cumulative data from three separate experiments, clinical disease began on day 9, 2 days before disease onset in the control mice, in the groups using glatiramer acetate in conjunction with either subcutaneous or ingested murine IFN-α (see Fig 2B). The maximal group clinical scores in all groups occurred at day 14 postimmunization. Control mice showed a mean maximal group clinical score equal to 2.4 ± 0.6 (SE). The glatiramer acetate group showed a mean maximal group clinical score equal to 1.53 ± 0.4 (SE), ingested IFN-α of 1.3 ± 0.6 (SE), subcutaneous IFN-α of 1.5 ± 0.6 (SE), glatiramer acetate and ingested IFN-α of 2.6 ± 0.3 (SE), and glatiramer acetate and subcutaneous IFN-α of 2.7 ± 0.2 (SE). Clinical scores were compared between groups by the Mann-Whitney rank sum test at days 12 through 17 postinoculation. Glatiramer acetate, subcutaneous murine IFN-α, and ingested murine IFN-α individually improved clinical scores significantly at days 13 and 14 compared with control ($p < 0.05$). In contrast, glatiramer acetate in conjunction with either subcutaneous or ingested IFN-α did not improve clinical scores on days 12 through 17 compared with control. These experiments demonstrate that a combination of either ingested or subcutaneous murine IFN-α in conjunction with glatiramer acetate abrogates the clinical effectiveness of either therapy. In several experiments, cytokine analysis of antigen- or mitogen-stimulated spleen cell IL-2, IL-4, IL-6, IL-10, tumor necrosis factor-α, transforming growth factor-β, or IFN-γ production demonstrated no significant differences in cytokine production between control mice and groups treated with either IFN-α, glatiramer acetate, or glatiramer acetate and IFN-α (data not shown).

Glatiramer acetate (copolymer-1) is a synthetic amino acid copolymer that inhibits the T-cell response to myelin basic protein, suppresses EAE in many animal species,[12] exhibits cross-reactivity with myelin basic protein, and shows a progressively polarized development toward the Th2 pathway by secretion of IL-4, IL-6, and IL-10. Glatiramer acetate T cells ameliorated EAE induced by two unrelated encephalitogenic epitopes of PLP: p139–151 and p178–191, suggesting bystander suppression as the mechanism of action.[13,14]

IFN-β, an immune modulator with no antigenic specificity, delays the onset and decreases the severity of EAE symptoms, inflammation, and demyelination.[15,16] The beneficial effect of IFN-β treatment in MS patients may be in part a result of its ability to decrease metalloproteinase-9 activity of T cells, which allows migration of activated T lymphocytes through the cerebral endothelium, leading to a reduction of CNS T-lymphocyte infiltration.[17]

In the intact animal model, the effect of parenteral or ingested IFN-α on metalloproteinase-9 could result in ablation of the therapeutic efficacy of glatiramer acetate by inhibition of glatiramer acetate Th2 T-cell lymphocyte infiltration into the CNS. It is proposed that these cells may need to gain access to the CNS to downregulate Th1-mediated tissue destruction. Glatiramer acetate may inhibit the activity of type I interferon by stimulating the production of IL-10 and IL-4 from responsive Th2 cells. IL-10 can directly inhibit STAT-dependent early-response gene expression induced by IFN-α by suppressing the tyrosine phosphorylation of STAT1, an important intermediary in type I interferon signal transduction.[18] IL-4 inhibits interferon-induced RNA levels by reducing the transcriptional activator, interferon-stimulated gene factor 3.[19] As a result, in the animals undergoing combined treatment, the benefits of either drug used alone are lost.

It is possible that the optimal IFN-α dose by mouth (10 IU) or by injection (100 IU) is not the optimal dose in conjunction with glatiramer acetate. We used a suboptimal dose of glatiramer acetate to determine the synergistic or deleterious effect of ingested or parenteral

IFN-α. The optimal dose of glatiramer acetate (10 mg) in conjunction with lower IFN-α doses may have demonstrated an additive or synergistic effect. Similarly, different timing of the introduction of the two drugs or use in a model of relapsing or progressive EAE after initial disease induction might result in a different outcome. Our inability to detect differences in proinflammatory of anti-inflammatory cytokine production between the glatiramer acetate, ingested and parenteral IFN-α groups, and control and combination groups may reflect the performance of assays at days 17 and 18, after peak group clinical disease differences had passed. Clinical trials designed to test a possible additive or synergistic effect of glatiramer acetate (Copaxone) and IFN-β (Avonex) in man should be designed to detect possible adverse effects of this combination of immunomodulatory agents.

This study was supported by a grant from Teva Pharmaceutical Industries, Israel.

References

1. Durelli L, Bongioanni MR, Cavallo R, et al. Chronic systemic high-dose recombinant interferon alpha-2a reduces exacerbation rate, MRI signs of activity, and lymphocyte interferon gamma production in relapsing-remitting multiple sclerosis. Neurology 1994;44:406–413
2. Interferon beta-1b is effective in relapsing-remitting multiple sclerosis. I. Clinical results of a multicenter, randomized, double-blind, placebo-controlled trial. Neurology 1993;43:655–661
3. Jacobs L, Cookfair D, Rudick R, et al. Intramuscular interferon beta-1a for disease progression in relapsing multiple sclerosis. The Multiple Sclerosis Collaborative Research Group (MSCRG). Ann Neurol 1994;39:285–294
4. Randomised double-blind placebo-controlled study of interferon beta-1a in relapsing/remitting multiple sclerosis. PRISMS (Prevention of Relapses and Disability by Interferon beta-1a Subcutaneously in Multiple Sclerosis) Study Group. Lancet 1998;352:1498–1504
5. Johnson KP, Brooks BR, Cohen JA, et al. Copolymer 1 reduces relapse rate and improves disability in relapsing-remitting multiple sclerosis: results of a phase III multicenter, double-blind, placebo-controlled trial. Copolymer 1 Multiple Sclerosis Study Group. Neurology 1995;45:1268–1276
6. Myhr KM, Riise T, Green Lilleas FE, et al. Interferon-alpha2a reduces MRI disease activity in relapsing-remitting multiple sclerosis. Norwegian Study Group on Interferon-alpha in Multiple Sclerosis. Neurology 1999;52:1049–1056
7. Lublin FD, Reingold SC. Combination therapy for treatment of multiple sclerosis [see comments]. Ann Neurol 1998;44:7–9 (Editorial)
8. Alvord EC, Shaw CM, Huby S, Kies MK. Encephalitogen-induced inhibition of experimental allergic encephalomyelitis: prevention, suppression, and therapy. Ann NY Acad Sci 1965; 122:333–345
9. Brod SA. Effect of oral administration of type 1 interferon on experimental autoimmune encephalomyelitis. In: Reder AT, ed. Interferon therapy in multiple sclerosis. New York, Marcel Dekker, 1996:245–286
10. Brod SA, Khan M. Oral administration of IFN-alpha is superior to subcutaneous administration of IFN-alpha in the suppression of chronic relapsing experimental autoimmune encephalomyelitis. J Autoimmun 1996;9:11–20
11. Lando Z, Teitelbaum D, Arnon R. Effect of cyclophosphamide on suppressor cell activity in mice unresponsive to EAE. J Immunol 1979;123:2156–2160
12. Lisak RP, Zweiman B, Blanchard N, Rorke LB. Effect of treatment with Copolymer 1 (Cop-1) on the in vivo and in vitro manifestations of experimental allergic encephalomyelitis (EAE). J Neurol Sci 1983;62:281–293
13. Aharoni R, Teitelbaum D, Sela M, Arnon R. Bystander suppression of experimental autoimmune encephalomyelitis by T cell lines and clones of the Th2 type induced by copolymer 1. J Neuroimmunol 1998;9:135–146
14. Teitelbaum D, Aharoni R, Arnon R, Sela M. Specific inhibition of the T-cell response to myelin basic protein by the synthetic copolymer Cop 1. Proc Natl Acad Sci USA 1988;85: 9724–9728
15. Abreu SL. Suppression of experimental allergic encephalomyelitis by interferon. Immunol Commun 1982;11:1–7
16. Yu M, Nishiyama A, Trapp BD, Tuohy VK. Interferon-beta inhibits progression of relapsing-remitting experimental autoimmune encephalomyelitis. J Neuroimmunol 1996;64:91–100
17. Stuve O, Dooley N, Uhm H, et al. IFNβ-1b decreases the migration of T lymphocytes in vitro–effects on matrix metalloproteinase-9. Ann Neurol 1996;40:853–863
18. Ito S, Ansari P, Sakatsume M, et al. Interleukin-10 inhibits expression of both interferon alpha– and interferon gamma–induced genes by suppressing tyrosine phosphorylation of STAT1. Blood 1999;93:1456–1463
19. Larner AC, Petricoin EF, Nakagawa Y, Finbloom DS. IL-4 attenuates the transcriptional activation of both IFN-alpha and IFN-gamma–induced cellular gene expression in monocytes and monocytic cell lines. J Immunol 1993;150:1944–1950

Intraoperative Unmasking of Brain Redundant Motor Sites during Resection of a Precentral Angioma: Evidence Using Direct Cortical Stimulation

Hugues Duffau, MD,* Jean-Pierre Sichez, MD,* and Stéphane Lehéricy, MD†

We report the first observation of real-time intraoperative evidence of a retrocentral redistribution of motor areas with an unmasking of precentral redundant motor sites, before and after, respectively, surgical removal of a precentral arteriovenous malformation using direct electrical stimulation. This study shows large-scale plasticity of the motor function behind the central sulcus as the result of an arteriovenous malformation, the brain's ability to effect short-term unmasking of precentral motor sites after arteriovenous malformation resection, and the existence of redundant precentral and postcentral motor areas for the same movement, suggesting that the central sulcus does not simply divide motor and sensory functions.

Duffau H, Sichez J-P, Lehéricy S. Intraoperative unmasking of brain redundant motor sites during resection of a precentral angioma: evidence using direct cortical stimulation. Ann Neurol 2000;47:132–135

Recent studies using functional neuroimaging methods have reported the existence of functional cerebral reorganization in arteriovenous malformation (AVM) cases,[1] as previously described in other congenital or slow-growing acquired lesions.[2,3] Moreover, the ability of the brain to redistribute the eloquent areas and pathways after acute injury or surgery has been observed.[4–6] The mechanisms of recovery still remain obscure, however, particularly for motricity, in spite of the hypothesis of an ipsilateral pyramidal tract recruitment[7] or a restoration system within the primary motor cortex (M1).[5]

We report the first observation of intraoperative evidence of a retrocentral redistribution of motor areas with an unmasking of precentral redundant motor eloquent sites before and after, respectively, surgical removal of a precentral AVM using direct cortical stimulation (DCS). The functional compensatory mechanisms are discussed on the basis of these findings.

Patient and Methods

This right-handed 39-year-old man presented with seizures and an otherwise normal neurological examination. A left precentral AVM was diagnosed on angiography and magnetic resonance imaging (MRI). Embolization was performed first; because of an inability to obtain complete obliteration (80% only), surgery was then undertaken.

Preoperative functional MRI (fMRI) using the blood-oxygen level–dependent technique was performed after AVM embolization, with mapping activations of the right and left motor cortex by repetitive movements of the opposite hand (self-paced flexion/extension). A discordance between the location of functional activations during the right-hand movements related to the identification of the central sulcus using anatomical criteria previously reported[8] was observed. Indeed, motor activations seemed to be found in the retrocentral gyrus as expected (Fig 1). The AVM was separated from eloquent sites by a gyrus without any activation visible by means of fMRI.

Surgery was performed under general anesthesia without curarization. After cortex exposure and before resection, motor cortical mapping was performed using DCS, with a 5-mm tipped bipolar probe, as already described.[9,10] Stimulation parameters were set at 60-Hz biphasic square wave pulses (1 msec per phase), with a 16-mA current amplitude (highest current nondeleterious for the brain) (Ojemann Cortical Stimulator; Radionics). Indeed, it is admitted that with these parameters, the absence of a motor response for one site after three nonconsecutive stimulations means that this site is not eloquent and can be resected without neurological sequelae, as confirmed by the clinical results.[9,10]

Motor responses were clinically evaluated without electromyographic recording. Three functional motor sites for arm and hand movements were found at the same location as that detected by means of fMRI, namely, separated from the AVM by a gyrus without any response to DCS (Fig 2). Confirmation of functionality for these three sites was obtained using three nonconsecutive stimulations, inducing the same movements each time in the same three areas (marked by numbered tags). All of the other areas of the exposed cortex were accurately stimulated without motor response.

The lesion was removed, with sequential repetitions (during and after resection) of DCS with equivalent parameters. The same three motor areas as those labeled before resection were identified by means of tags and stimulated with the same motor response, showing that the pre- and postremoval DCS maps were reproducible. Moreover, two new functional sites were detected that induced the same hand and arm motor responses but were located in the gyrus in front of the previous eloquent region (ie, immediately behind the AVM). This gyrus corresponded to the supposed precentral gyrus (identified by means of anatomical criteria) for which no motor response was induced by means of DCS before AVM

From the Departments of *Neurosurgery 1 and †Neuroradiology, Hôpital de la Salpêtrière, Paris, France.

Received Jan 26, 1999, and in revised form Jul 1 and Aug 23. Accepted for publication Aug 27, 1999.

Address correspondence to Dr Duffau, Service de Neurochirurgie 1, Hôpital de la Salpêtrière, 47 Boulevarde de l'Hôpital, 75651 Paris, Cedex 13, France.

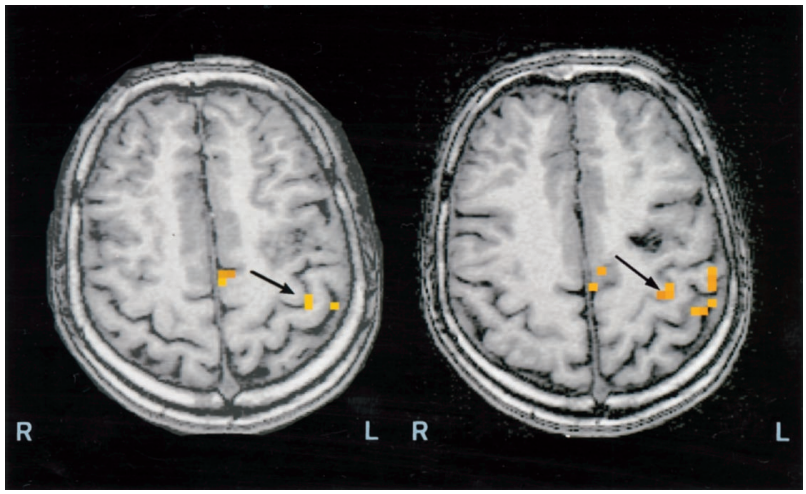

Fig 1. Anatomical MRI showing left precentral arteriovenous malformation (AVM) with superimposed functional MRI (carried out by means of 1.5-T MRI using the blood-oxygen level–dependent method during right-hand movement). Motor activations were obtained in and behind the anatomically presumed central sulcus (arrow) *but not close to the AVM as expected. We also noted activations in the left supplementary motor area. L = left; R = right.*

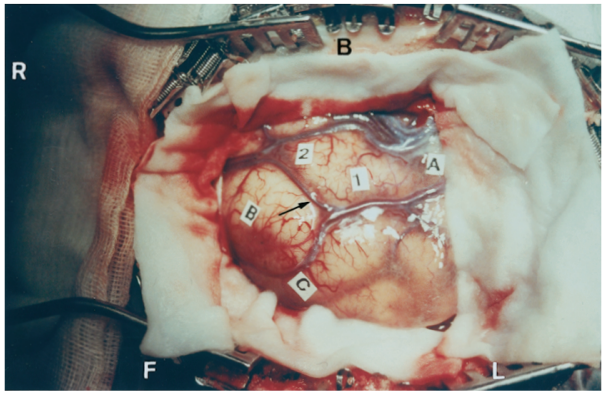

Fig 2. Intraoperative view before surgical resection. Motor areas were mapped using direct cortical stimulation. Medially to laterally, the motor arm site (2), the motor hand site (1), and the motor finger sites (A) are indicated; the arteriovenous malformation (AVM) boundaries are also delineated (B and C). As demonstrated by preoperative functional MRI, we found a sulcus (arrow) *and a gyrus without motor response between the functional areas and the AVM during surgery; the "precentral" gyrus was defined using anatomical but not functional criteria. F = forward; B = backward; L = left; R = right.*

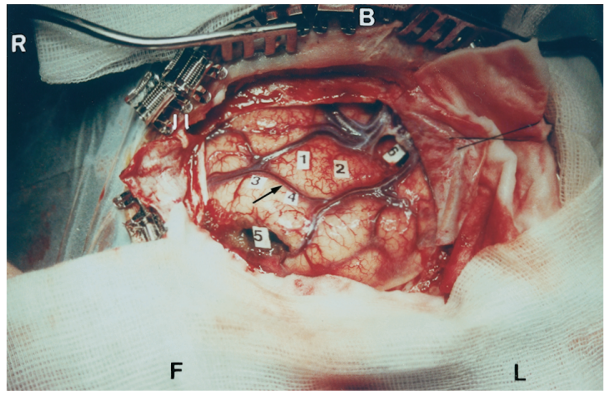

Fig 3. Intraoperative view after arteriovenous malformation (AVM) removal. New motor mapping using the same electrical parameters shows the following: (1) The same motor areas as in the preoperative mapping. For technical reasons, the numbers 1 and 2 are inverted on this photograph; tag 1 now represents the motor arm site, and tag 2 represents the motor hand site. Tag 6 was used instead of the letter A to indicate the motor finger area. (2) Detection of two new and redundant motor areas in front of the sulcus (arrow) *and in the "anatomical" precentral gyrus. Stimulation of the site marked by tag 3 induces the same arm movement as that elicited by stimulation of the site marked by tag 1, and stimulation of the site marked by tag 4 induces the same hand movement as that elicited by stimulation of the site marked by tag 2. (3) Confirmation that functional motor pyramidal tracts exist immediately behind the AVM by inducing a motor hand response using subcortical stimulation (ie, at the level of the posterior edge of the surgical cavity) marked by tag 5. F = forward; B = backward; L = left; R = right.*

resection. Using subcortical stimulation, which gave motor responses on the posterior edge of the surgical cavity (Fig 3), total AVM removal with respect to the functional tissue was achieved.

The patient presented with an immediate postoperative arm motor deficit, which was likely a result of both local hemodynamic modifications and edema, with complete recovery in 1 month. No functional exploration was performed after surgery.

Discussion

Dynamic sensorimotor cortical plasticity for functional reorganization in man has been illustrated in cases of congenital malformations (ie, AVMs,[1] neonatal lesion[2]) and acquired injuries (ie, stroke,[6] tumors[3,5]) or after surgery.[4] Several mechanisms of recovery have been advocated, particularly recruitment of the ipsilateral pyramidal tract[7] or parallel projection systems from adjacent motor cortical areas.[6] These mechanisms work by means of neurofunctional imaging methods performing

"instantaneous" brain mapping but did not incorporate a study of functional organization immediately before and after the occurrence or disappearance (in the case of surgery) of the lesion.

Our report allows a dynamic real-time study of the redistribution of cortical motor areas during the surgical resection of a precentral AVM using preoperative fMRI and overall intraoperative DCS, which represents a safe, reliable, and accurate technique of brain mapping.[9,10] Indeed, although hemodynamic characteristics of the AVM may induce some interference with the blood-oxygen level–dependent technique used for fMRI,[11] the sensibility and specificity of DCS have already been reported in this pathology,[12] as a result of their electrophysiological (and not directly hemodynamic-dependent) mechanism of functional detection. Moreover, the accuracy of DCS, without any cortical diffusion, has already been demonstrated using optical imaging.[13] Nowadays, it is well established that each site inducing movement during three nonconsecutive DCSs (to avoid a refractory state) represents an eloquent area that must be preserved and functionally tested after resection.[9,10] If DCS after resection produces the same movement that it produced before resection, there is no postoperative motor deficit; if it does not, there is paralysis. Furthermore, all regions without response during DCS before resection (at the higher current intensity of 16 mA) can be removed without postoperative sequelae.

To our knowledge, there is no report of the appearance of new eloquent sites detected by DCS before and after resection. Our data suggest the existence of a compensatory mechanism of reorganization of the motor areas in the retrocentral gyrus, which is likely a result of the congenitodevelopmental nature of the AVM, with an excellent concordance between fMRI and pre-resection DCS results. This observation supports the findings of Seitz and co-workers,[5] who advocated (using positron emission tomography) a large-scale reorganization beyond the limits of M1 (particularly dorsal to the postcentral sulcus) in cases of slowly growing tumors.

Moreover, our data demonstrated a short-term unmasking of redundant cortical motor areas in the precentral gyrus immediately after AVM removal, with multiple pre- and post-Rolandic cerebral representations of the same movements becoming detectable. This observation of multiple cortical representations for the same motor function has already been described in normal human subjects using fMRI,[14] but it was seen exclusively within the precentral region and not with redundant motor sites behind and in front of the central sulcus. These findings are likely explained by the mechanism of the masking of precentral "primary" motor areas during the development of the AVM, with simultaneous unmasking of preexisting postcentral areas as a result of the desinhibition or sprouting of new axon terminals to postcentral areas.[15] Indeed, experimental studies have already suggested that an area of the cerebral cortex is able to assume the role of another area.[16] Thus, it is conceivable that the hand movements in our patient were made possible by remapping of motor functions from their original site to functionally normal retrocentral regions, suggesting a compensatory motor function of the somatosensory cortex for the motor cortex impaired by cooling (according to the data reported in a primate model).[17] One explanation would be that both of the circuits (including the motor and somatosensory cortex) are capable of sustaining motor function normally (morphological studies in primates showed that nearly half of the pyramidal tracts originate in the postcentral primary sensory cortex [S1]) with a predominance of the precentral circuit and some assistance by S1, which may be a result of the fact that the M1 circuit precedes that of the S1 in action. The action of S1 becomes predominant for movement execution when M1 is not functioning; in our case, it was a result of the inhibition caused by the AVM. Our data thus tend to confirm, as previously reported by Nii and colleagues,[18] that motor and sensory hand cortices overlap and are not divided in a simple manner by the central sulcus.

The short-term appearance of motor function in the precentral gyrus after AVM resection does not seem to be explainable by a sole hemodynamic mechanism, as 80% of the AVM was embolized prior to resection. The hypothesis of a local mechanism coupled with a biochemical mechanism may be evoked: it is likely that the disappearance of the mass induces short-term changes in synaptic efficacy or switches on local network properties on the same basis that has already been shown for cortical lesions (with traumatic and metabolic effects), which are able to induce disturbances in the GABA-ergic receptors,[19] resulting in M1 rapid mapping modifications as a result of the suppression of local inhibition.[15,20]

Conclusions

This observation provides some evidence in favor of the existence of brain plasticity as determined by means of DCS. First, large-scale plasticity of motor function behind the central sulcus as a result of a congenital precentral AVM is demonstrated. Second, the ability of the brain to effect short-term unmasking of precentral motor sites after lesion resection is observed. Third, redundant pre- and postcentral motor areas have been detected for the same function, suggesting that the central sulcus does not simply divide motor and sensory functions.

References

1. Maldjian J, Atlas SW, Howard RS, et al. Functional magnetic resonance imaging of regional brain activity in patients with

intracerebral arteriovenous malformations before surgical or endovascular therapy. J Neurosurg 1996;84:477–483
2. Lewine JD, Astur RS, Davis LE, et al. Cortical organization in adulthood is modified by neonatal infarct: a case study. Radiology 1994;190:93–96
3. Wunderlich G, Knorr U, Herzog H, et al. Precentral glioma location determines the displacement of cortical hand representation. Neurosurgery 1998;42:18–27
4. Mogilner A, Grossman JAI, Ribary U, et al. Somatosensory cortical plasticity in adult humans revealed by magnetoencephalography. Proc Natl Acad Sci USA 1993;90:3593–3597
5. Seitz RJ, Huang Y, Knorr U, et al. Large-scale plasticity of the human motor cortex. Neuroreport 1995;6:742–744
6. Weiller C, Chollet F, Friston KJ, et al. Functional reorganization of the brain in recovery from striatocapsular infarction in man. Ann Neurol 1992;31:463–472
7. Benecke R, Meyer BU, Freund HJ. Reorganization of descending motor pathways in patients after hemispherectomy and severe hemispheric lesions demonstrated by magnetic brain stimulation. Exp Brain Res 1991;83:419–426
8. Yousry TA, Schmid UD, Alkhadi H, et al. Localization of the motor hand area to a knob on the precentral gyrus: a new landmark. Brain 1997;120:141–157
9. Berger MS, Ojemann GA. Intraoperative brain mapping techniques in neuro-oncology. Stereotact Funct Neurosurg 1992;58: 153–161
10. Ojemann GA, Ojemann JG, Lettich E, Berger MS. Cortical language localization in left, dominant hemisphere: an electrical stimulation mapping investigation in 117 patients. J Neurosurg 1989;71:316–326
11. Beltramello A. Motor cortex activation in a patient with arteriovenous angioma in the left region. Intervent Neuroradiol 1996;2:155–156
12. Burchiel KJ, Clarke H, Ojemann GA, et al. Use of stimulation mapping and corticography in the excision of arteriovenous malformations in sensorimotor and language-related neocortex. Neurosurgery 1989;24:322–327
13. Haglund MM, Ojemann GA, Blasdel GG. Optical imaging of bipolar cortical stimulation. J Neurosurg 1993;78:785–793
14. Sanes JN, Donoghue JP, Edelman RR, Warach S. Shared neural substrates controlling hand movements in human motor cortex. Science 1995;268:1775–1777
15. Jacobs KM, Donoghue JP. Reshaping the cortical motor map by unmasking latent intracortical connections. Science 1991; 251:944–947
16. Castro-Alamancos MA, Garcia-Segura LM, Borrell J. Transfer of function to a specific area of the cortex after induced recovery from brain damage. Eur J Neurosci 1992;4:853–863
17. Sasaki K, Gemba H. Compensatory motor function of the somatosensory cortex for the motor cortex temporarily impaired by cooling in the monkey. Exp Brain Res 1984;55:60–68
18. Nii Y, Uematsu S, Lesser RP, Gordon B. Does the central sulcus divide motor and sensory functions? Cortical mapping of human hand areas as revealed by electrical stimulation through subdural grid electrodes. Neurology 1996;46:360–367
19. Eysel UT. Perilesional cortical dysfunction and reorganization. In: Freund HJ, Sabel BA, Witte OW, eds. Brain plasticity. Advances in neurology, vol 73. Philadelphia: Lippincott-Raven, 1997:195–207
20. Donoghue JP. Plasticity of adult sensorimotor representations. Curr Opin Neurobiol 1995;5:749–754